Eliminate P-wave Direction in Application of Exploration Seismology

by

Vikri Januarisma

Dissertation submitted in partial fulfillment of

the requirement for the

Bachelor of Engineering (Hons)

(Electrical and Electronics Engineering)

JANUARY 2016

Universiti Teknologi PETRONAS

Bandar Seri Iskandar

31750 Tronoh

Perak Darul Ridzuan

CERTIFICATION OF APPROVAL

Eliminate P-wave Direction in Application of Exploration Seismology

by

Vikri Januarisma

A project dissertation submitted to the

Electrical and Electronics Engineering Programme

Universiti Teknologi PETRONAS

in partial fulfillment of the requirement for the

Bachelor of Engineering (Hons)

(Electrical and Electronics Engineering)

Approved by,

_____

(Dr. Dennis Ling Chuan Ching)

UNIVERSITI TEKNOLOGI PETRONAS

TRONOH, PERAK

January 2016

CERTIFICATION OF ORIGINALITY

This is to certify that I am responsible for the work submitted in this project, that the original work is my won except as specified in the references and acknowledgements, and that the original work contained herein have not been undertaken or done by unspecified sources or persons.

_____

(Vikri Januarisma, ID: 17791)

ABSTRACT

Exploration seismology has substantially contributed to finding and developing giant field worldwide. The technology has evolved in single to two, three dimensional methods, and later added a fourth dimension for reservoir monitoring [1]. In land seismic acquisition, a variety of innovative single, three or multiple geophone has been developed by some manufacturer. In this project, the experiment will demonstrate numerous applications for single component geophone (SM – 24) using different composition of sand and rock proportion. The source vibration will generate by a geophone (SM-24) which supplied external frequency from the function generator. The resulting output by single component geophone only provides the output voltage of the propagating elastic wave in one direction.

ACKNOWLEDGEMENT

This dissertation would not have been successfully completed without the guidance and the help of several individuals who in one way or another contributed and extended their valuable assistance in the preparation and completion of this study.

First and foremost, I wish my utmost gratitude to my supervisor, Dr Dennis Ling Chuang Ching who was abundantly helpful and offered invaluable assistance, support and guidance.

Precious thanks to UTP Research Center as this project is sponsored by UTP Research Center. I would also like to convey thanks to the all the Geophysics lab technicians for all the help and assistance.

Last but not the least, I wish to express my love and gratitude to my beloved families; for their understanding and support, throughout the duration of my studies.

TABLE OF CONTENTS

LIST OF FIGURES

LIST OF TABLES

CHAPTER 1
INTRODUCTION

1.1 BACKGROUND

In two decades, single component geophone has been used in exploration seismology. For instance, seismic exploration for hydrocarbon starts by emitting a compressional P – wave using vertical vibrational truck or dynamite [1]. P – wave displacement directed the wave travel that record vertically travelling waves with geophones that are sensitive to particle displacement in the vertical direction, and S – wave recorded horizontally by geophone termed as radial, if the horizontal Geophone record displacement in the direction of the seismic line [2]. Thus, P – wave has ability to determine the rock rigidity, density and compressibility compared with S – wave that more sensitive only to the rock rigidity and density.

Since the beginning of seismic exploration, conventional coil geophone has been used as the standard sensor until the end of 1980's it developed into inexpensive source of converted S – wave [3]. Prior to the ability of single geophone that only provides propagating elastic wave in one direction, the three component geophone is used to overcome these problems. It estimated the direction of incidence from three component geophone becomes possible to enhance arrivals from only around the reflector point on the qui – travel time plane [4]. Moreover, an application of single component can be applied in three component geophones to enhance the capability of receiving three different waves in a vertical, radial, and transverse signal in future implementation.

Application of three component geophones applied in Vertical Seismic Profiling (VSP). Vertical Seismic Profiling (VSP) is a measurement in which a seismic signal generated at the surface of the earth is recorded by geophones secured at various depths to the wall of a drilled well [5]. VSPs have higher resolution than surface seismic recordings prior to the seismic wave mostly pass through the attenuating near surface layers solitary once, which is not the case with surface recorded data. Moreover, the ability to spread a seismic wave in VSPs will indicate the down going

and up going wavefields and reflected at a boundary of the layers that will record on the surface by a receiver of geophones.

1.2 PROBLEM STATEMENT

Conventional geophone (SM-24) has fixed parameter to 28.8 V/m/s approximately to 0.73V/in/s sensitivity given for single component directional parameters (x or y). The horizontal or vertically aligned elements are velocity waveform of the single source where the recorded data is overlapping among each other. Thus, different sensitivity elements are needed for each horizontal or vertical aligned elements.

1.3 OBJECTIVE

Based on problem statement above, the objectives need to achieve at the end of the project is to eliminate the P-wave direction in application of material references being used.

1.4 SCOPE of STUDY

Several scope of study to achieve the project described as below;

- The source of vibration will perform using Function Generator
- The measurement reading will perform using Digital Oscilloscope

CHAPTER 2
LITERATURE REVIEW

2.1 VERTICAL SEISMIC PROFILING

Vertical Seismic Profiling (VSP) has been applied to many locations over the world for the exploration ahead of the tunnel or related application [6]. In exploration seismology, understanding of wave propagation is an important point and hence seismic modeling is an important tool [7]. For instance, VSP is important to provide seismic and borehole image. It allows the user to create detailed velocity profiles, and assist with an advanced exploration techniques such as imaging below the drill bit, and allow user to accurately estimate anisotropy parameters. In term of physical characteristics, VSPs recorded both down going and up going wavefields. Moreover, to process the VSP to involve in separating the wavefields and identifying the primary events, the user interprets the VSP at each processing step to obtain an understanding of the wavefields.

The most common type uses for VSPs are downhole receivers and a surface source. In a single or three component Geophones, the VSP used is downhole receivers [2]. During crosswell surveying in figure 1, some of the receivers contain the array elements containing either a single components or three component Geophones. Those receivers are located within a single tool at each level, and the receiver space within a two can carry the certain distance as user expected. Hence, the receiver spacing and the number of the level indicated as how the survey will be conducted. If the survey required many receiver depths to be recorded, the use of a short level tool (e.g five level) can be affected to the time consuming processes.

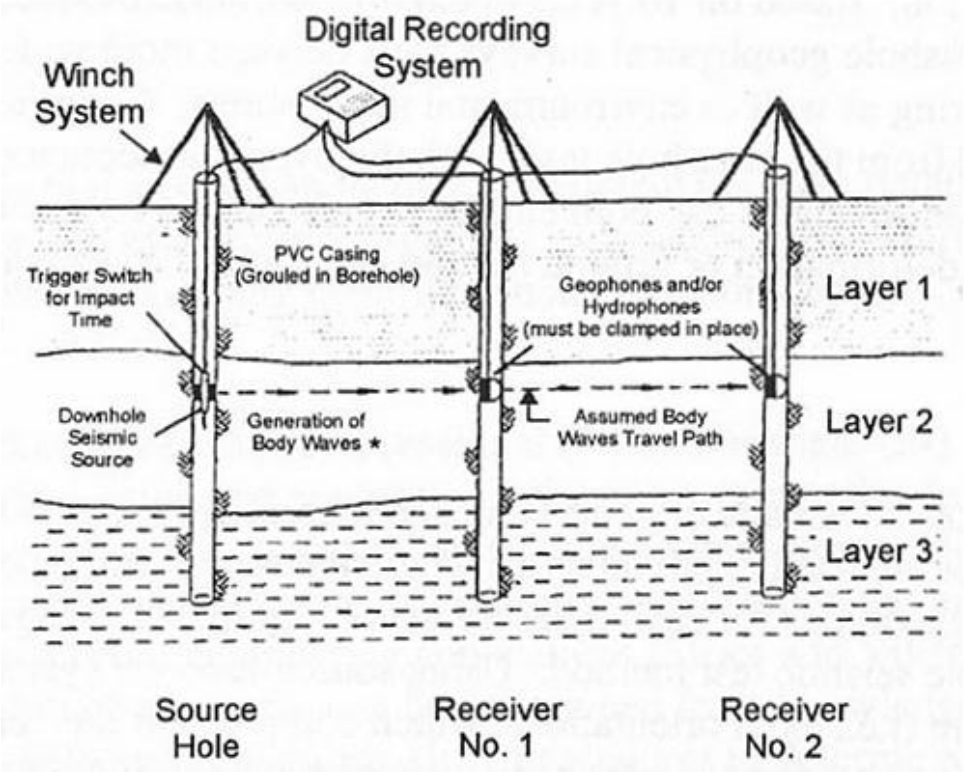

Figure.1. Crosswell surveying

Based on figure 1, the method depends upon the source type of seismic wave that generated as P wave, S wave or SH body waves. However, the crosswell method helps Geophones to provide the detail information of each seismic wave velocity between the closely spaced boreholes [8].

In this method, geophones are anchored to the borehole wall at known depths in the well, and measurements are made of the arrival time of a seismic wave emitted by a surface source. Velocity of geophone anchored to the borehole wall receives information coming from two opposite direction up-going and the down-going wavefields and reflected wavefields. At the number of receiver positions in the well, the signal is recorded by a geophone continuously based on each level position. As a function of time, at each level the recorded signal will contain first the primary down-going signal from the source and any multiples generated at the surface. At the end, both of down going and up going wavefields functioned to produce the output voltage proportionally to the velocity of geophones.

2.2 GEOPHONES

Geophones have been impacted valuable to the industry for more than five decades. Geophones are the first link in the seismic recording field system [9]. Thus, geophone has empowered enable a multiplicity of industry within a simple reliable design. In conventional seismic surveying, the seismic signals detected by geophones are recorded as amplitude variations along the time axis. Common depth point stacking, which is conventionally used in the reflection seismic method provides approximate sub – surface velocities for depth conversion [4]. For instance in the case of head of tunnel, in order to estimate the location of a reflector ahead of the tunnel face, it is necessary to image the geology using the variation of amplitude with distance from the face [10].

In generally, the function of geophone is to produce with the utmost fidelity an electrical analogue of the vertical component of ground motion. Most of the geophones used in land seismic explorations today are electromagnetic type. In electromagnetic geophone, the magnets is coupled to the ground and for practical purposes move into it, while the suspended coil and its former due to their inertia and tend to remain stationary. Basically, the relative movement between the coil and magnet causes a voltage to be generated across the windings of the coil. This voltage is proportional to the rate at which the coil cuts the magnetic flux to its velocity with respect to the sensitivity. The sensitivity of a typical reflection geophone at 0.7 critical damping is of the order of 10V/m/s. Therefore, an output of 0.1 μ geophones requires a ground displacement of $0.1x10^{-7}$/m/s [11].

In modern geophones, the electromagnetic damping is used. A voltage is generated across the geophone coil when its conductors cut the magnetic flux. So that, it created a force which always opposes the coil's movement. If the frequency is increased above the natural frequency, the excursion of the coil diminished. The natural resonant frequenct of moving system is given by the equation.

$$\frac{1}{2\pi}\sqrt{\frac{K}{m}} \quad ..(1)$$

where K= spring stiffness

M= suspended mass of coil

The displacement frequency curve of geophone can be translated into the amplitude – frequency response curve. The fundamental equation of motion for the electromagnetic geophone is derived by first determining the electrical current generated and substituting its relation into the basic force equation. The equation given by the expression;

$$M\frac{d2x}{dt2} + \left(D + \frac{G2}{(2.54)2(r+R)10-7}\right)\frac{dx}{dt} + Kx = -M\frac{d2y}{dt2} \quad \ldots. (2)$$

where M = mass of the coil

x = displacement of coil relative to case in cm

y = displacement of case relative to a fixed point in cm

D = damping factor due to friction

k = stiffness constant of spring

G = intrinsic voltage sensitivity in V/cm/s

R = load resistance in ohms

r = coil winding resistance in ohms

t = time in seconds

From basic equation (1) can be simplified by the following assumptions:

- The reactance of the coil is small
- The load is pure resistance
- The operation of the geophone is in the linear region
- The case displacement y is sinusoidal

The case displacement y, can be given by the expression:-

$$y = A \cos(\omega t + \theta)$$

where A = peak amplitude of case displacement

ω = driving frequency in radians

The main problem involved in the design and use of the geophones is to take full account of its characteristics that will enable the desired seismic waves to be

recorded with maximum clarity. High resistance connection between the geophone and recording amplifiers introduce noise and increase susceptibility to pick up from electrical power lines. The important parameters in geophone are intrinsic sensitivity, power to weight ratio, resonant frequency, open circuit damping, damping characteristics under loaded conditions and coil dc resistance [11].

Sensitivity is the amplitude quotient of the geophone output voltage and the ground velocity. It measured in volts per inch or centimeter per second. The method to test geophone is done by measuring several parameters at one time or individual parameter. In the case of three component geophones application, the efficacy of three component data is examined by comparison with a single – component data [4]. However, determining the travel time of a reflected waveform a single record is difficult and time consuming. Poor accuracy is also a considerable serious problem, particularly for records with poor S/N ratios.

In this project, the method used for measuring is testing the condition of geophone by different medium proportion. The geophone requires external vibration to perform the detection. Furthermore, single component geophone used as a vibration source during the testing by injected an external frequency from function generator.

2.3 SEISMOGRAPH

Seismograph read the earth's motion when the sledgehammer is measured in terms of movement relative to some object that remains independent of the ground motion. The object is a Geophone which consists of a mass suspended on springs within a case. During the sledgehammer précised, the mass remains still when the case around it moves with the ground. As it moves, Geophone recorded displacement of case relative to the mass as an information change with time.

Vertical Seismograph is being used to read output voltage that proportionally with velocity which has been recorded from Geophone. In this project, the Geophone is designing and testing from normally single component to three components. Therefore, multiple channel output from geophones required to have a multiple input for velocity seismograph.

CHAPTER 3
METHODOLOGY

3.1 PROJECT FLOW CHART

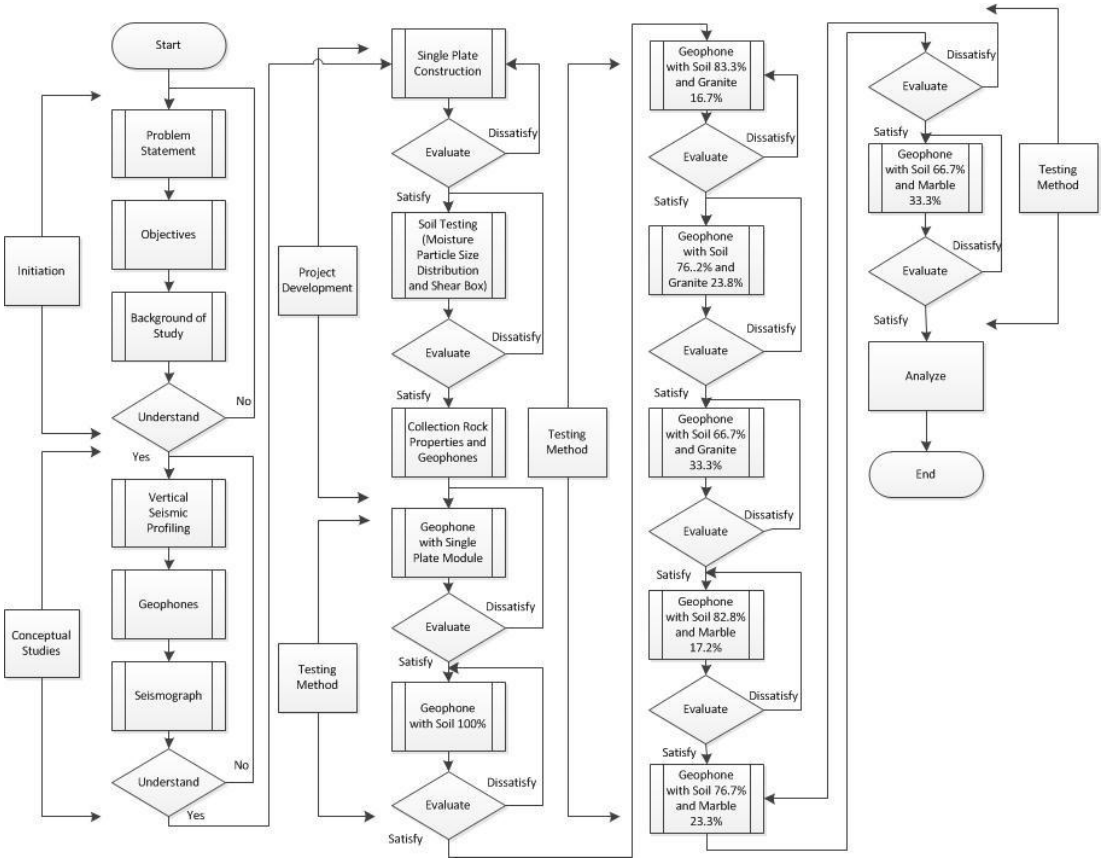

Figure.2. Flow chart final year project

3.2 PROJECT IDENTIFICATION

The project started from the second week of semester September 2015. The stage divided into two stages;

- **Conceptual studies**

Problem statement, objective, and scope of study are included into initialization stage. Specifically, to know further detail of design concept and method developed are discussed about vertical seismic profiling, geophones, and seismograph. Since

geophone is the devices which carry this project, hence the specific study concentrates more into geophone. Study concentrated in their specification, such as natural frequency, tolerance, distortion, damping ratio, sensitivity, coil resistance, and physical characteristics.

After the study has been taken, the selection of tools and equipment can be selected under project and development stage. This project looks into output voltage respectively with some vibration external. Therefore, oscilloscope, function generator and power supply are used to conduct the testing method. During the testing of geophone, it is going to compare between development of using step down converter and direct connection. As a result, additional of step down buck converter are used to carry this project with attached under appendix for the design.

- **Project development**

After first stage has been completed, the project moves forward to the second stage which is project development. In this stage several testing has to be conducted are;

- Soil testing method

Soil is a reference medium for conducting three elements of geophone SM-24. Soil reference tested for several methods such as;

- ✓ Moisture testing
- ✓ Particle size distribution testing
- ✓ Shearing box testing

Each of above testing will display the result in chapter 4 for result and discussion.

- Single plate design

Single plate is a medium to conduct single elements of geophone SM-24 while it tested together with function generator, oscilloscope and step down buck converter. The use of this plate to be a medium of vibration while the other geophone which act as the dynamo send a vibration signal through the other geophone. The design of plate shown in figure 4.

- Design and testing single element of geophone SM-24 without step down buck converter for measuring three different distance 5cm, 10cm, and 15cm

The method of conducting test for this stage is shown in figure 4.

- Design and testing single element of geophone SM-24 with step down buck converter for measuring three different distance 5cm, 10cm, and 15cm

The method of conducting test for this stage is shown in figure 4.

- Design and testing single element of geophone SM-24 without step down buck converter using material references (soil and rock properties)

The method of conducting test for this stage is shown in figure 4 but with additional soil or rock shown in figure 27.

- Design and testing single element of geophone SM-24 with step down buck converter using material references (soil and rock properties)

The method of conducting test for this stage is shown in figure 4 but with additional soil or rock shown in figure 27.

3.3 TOOLS and EQUIPMENT

- Conventional Geophones (SM-24)
- Digital Oscilloscope
- Function Generator
- Step down DC/DC Converter
- Plastic plate
- Soil references
- Rock references

3.4 GANTT CHART and MILESTONES

ID	Task Name	Start	Finish	Duration
1	**Final Year Project 1**	22/09/2015	10/12/2015	58d
2	**Initiation**	22/09/2015	09/10/2015	14d
3	Project Titled	29/09/2015	29/09/2015	1d
4	Problem Statement	30/09/2015	06/10/2015	5d
5	Objectives and Scope of Study	06/10/2015	09/10/2015	4d
6	**Conceptual Studies**	12/10/2015	06/11/2015	20d
7	Vertical Seismic Profiling	12/10/2015	21/10/2015	8d
8	Geophone	22/10/2015	28/10/2015	5d
9	Seismograph	29/10/2015	06/11/2015	7d
10	**Project Development**	09/11/2015	23/11/2015	11d
11	Single Plate Construction	09/11/2015	10/11/2015	2d
12	Soil Testing (Moisture, Particle Size Distribution, and Shearing Box Testing)	11/11/2015	20/11/2015	8d
13	Collected Rock Properties and Geophones	23/11/2015	23/11/2015	1d
14	**Testing Method**	24/11/2015	25/03/2016	89d
15	Geophone with Single Plate Module	24/11/2015	10/12/2015	13d
16	**Research Writing**	22/09/2015	27/11/2015	49d
17	Research Seminar (Plagiarism, Turnitin Briefing and Bibliographic)	28/09/2015	28/10/2015	23d
18	Submission (Extended Proposal, Proposal Defense, Interim Report)	19/10/2015	27/11/2015	30d

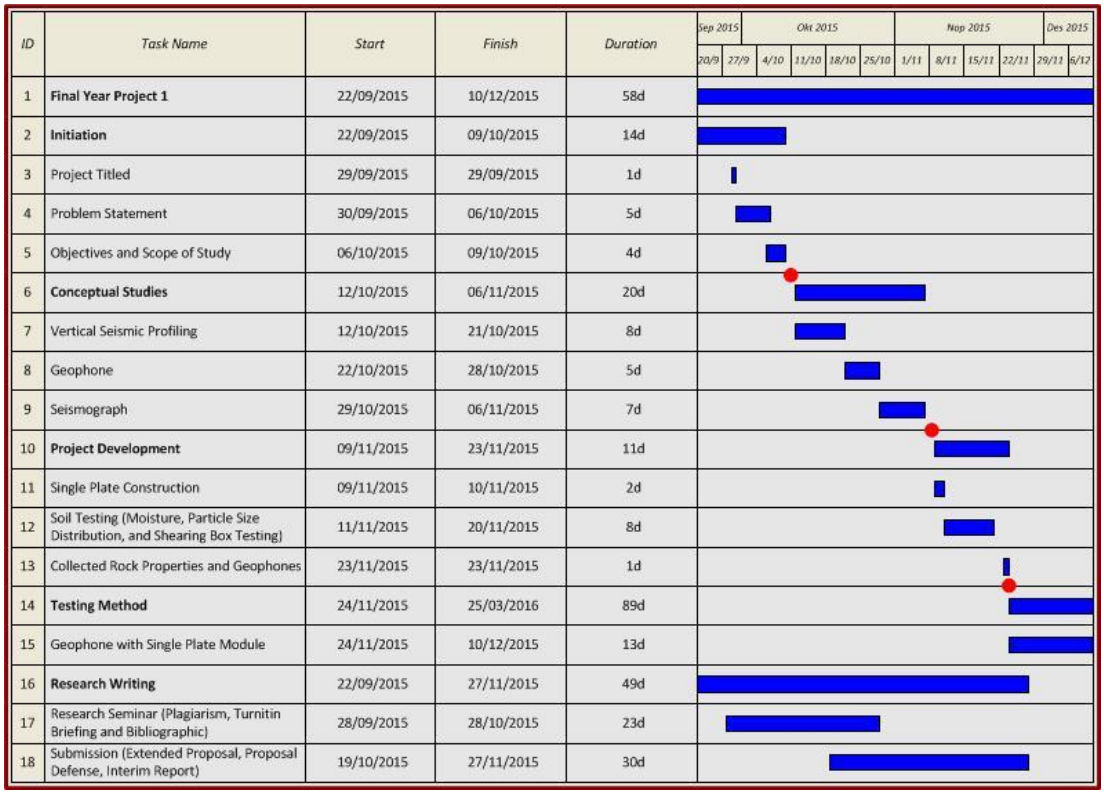

ID	Task Name	Start	Finish	Duration
1	**Final Year Project 2**	04/01/2016	26/05/2016	104d
2	**Testing Method**	04/01/2016	25/03/2016	60d
3	Geophone with Soil 100%	04/01/2016	20/01/2016	13d
4	Geophone with Soil 83.3% and Rock Granite 16.7%	21/01/2016	03/02/2016	10d
5	Geophone with Soil 76.2% and Rock Granite 23.8%	04/02/2016	16/02/2016	9d
6	Geophone with Soil 66.7% and Rock Granite 33.3%	17/02/2016	26/02/2016	8d
7	Geophone with Soil 82.8% and Rock Marble 17.2%	29/02/2016	09/03/2016	8d
8	Geophone with Soil 76.7% and Rock Marble 23.3%	10/03/2016	16/03/2016	5d
9	Geophone with Soil 66.7% and Rock Marble 33.3%	16/03/2016	25/03/2016	8d
10	**Research Writing**	22/01/2016	25/05/2016	89d
11	Research Seminar (Poster Presentation)	28/03/2016	28/03/2016	1d
12	Poster Presentation	30/03/2016	01/04/2016	3d
13	Viva Presentation	27/04/2016	27/04/2016	1d
14	Submission (Progress Report, Technical Paper, Draft Final, Dissertation)	11/03/2016	26/05/2016	55d

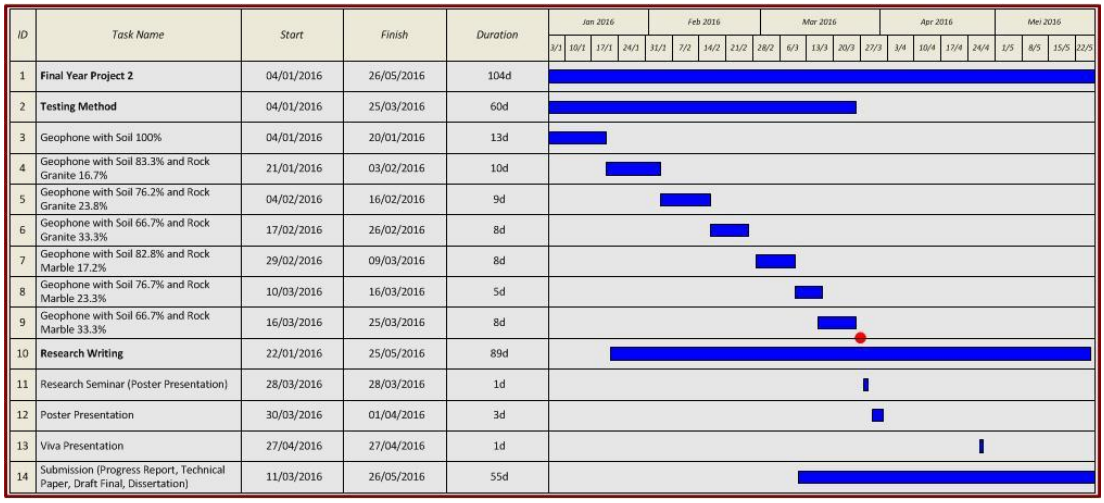

Figure.3. Gantt chart final year project

CHAPTER 4
RESULT AND DISCUSSION

4.1 PROGRESS SUMMARY

4.1.1 Soil Testing Method

There are three testing conducted for soil reference. Below are the types of the testing method;

- ✓ Moisture Testing
- ✓ Particle Size Distribution
- ✓ Shearing Box Testing

An above method conducted in lab soil testing. The objective of the testing is to see the composition moisture inside the soil and size particle of soil reference. The soil reference taken in Seri Bota, Ipoh with specification of sample type is core sample of soil.

4.1.2 Design Single Plate Module

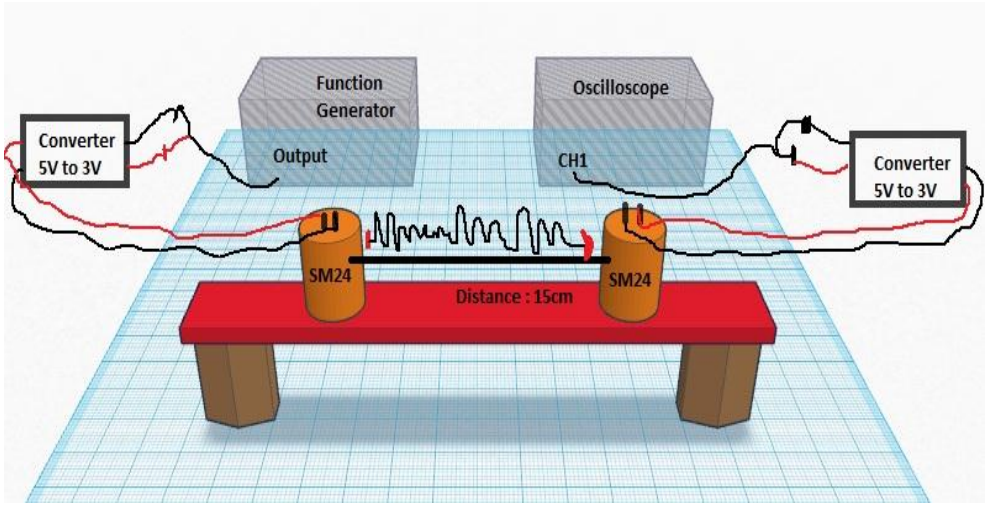

Figure.4. Overall sketch design of Conventional Geophone SM-24 for measurement output voltage within distance 15 cm

4.1.3 Software Design

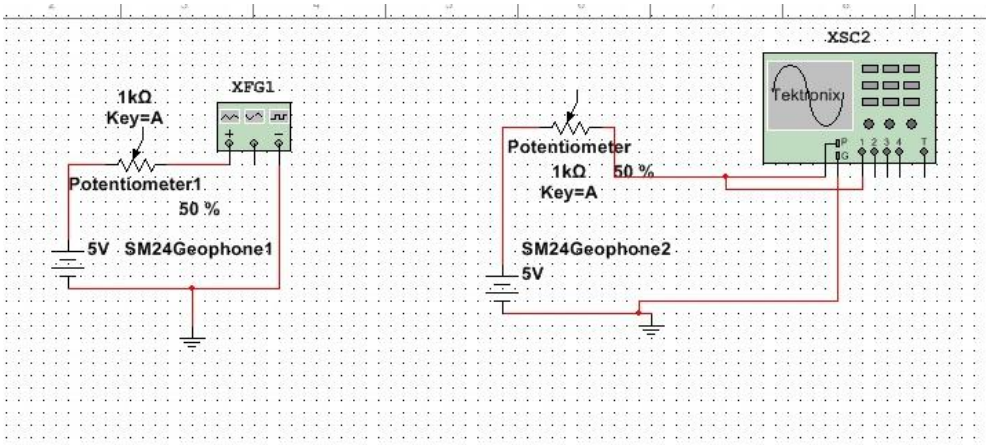

Figure.5. Overall design of Conventional Geophone SM-24 for measurement output voltage with potentiometer 1kΩ

4.2 FINDINGS

4.2.1 Software Result

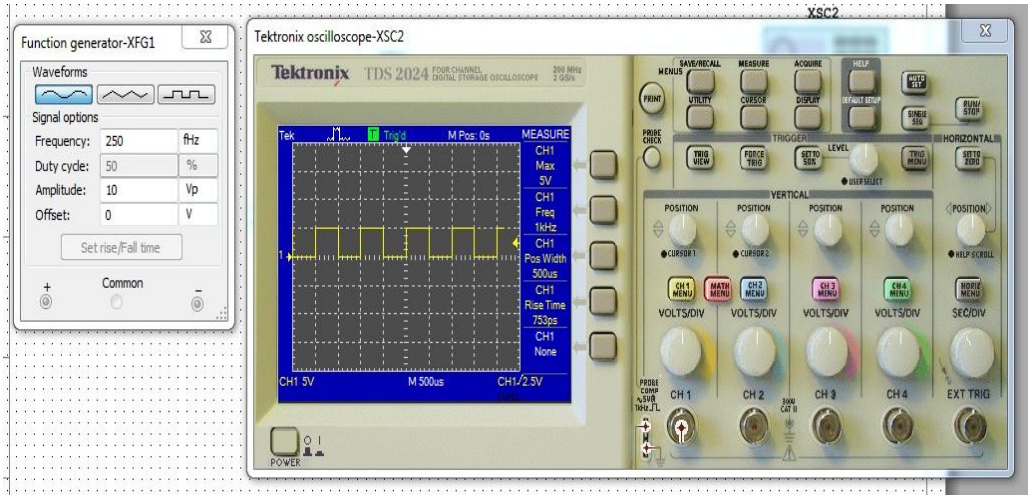

Figure.6. Output findings from design of Conventional Geophone SM-24 with potentiometer 1kΩ

4.2.2 Actual Measurement Result

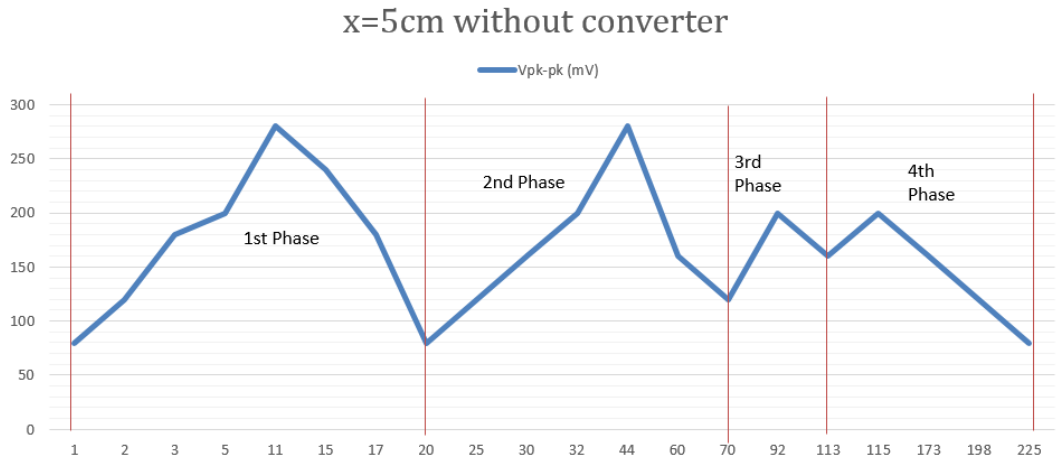

Figure.7. Output findings from sketch design of Conventional Geophone SM-24 for distance 5 cm without the step down buck converter

x=5cm	Frequency																			
Vpk-pk (mV)	1	2	3	5	11	15	17	20	25	30	32	44	60	70	92	113	115	173	198	225
Findings	80	120	180	200	280	240	180	80	120	160	200	280	160	120	200	160	200	160	120	80

Table.1. Output findings from sketch design of Conventional Geophone SM-24 for distance 5 cm without the step down buck converter

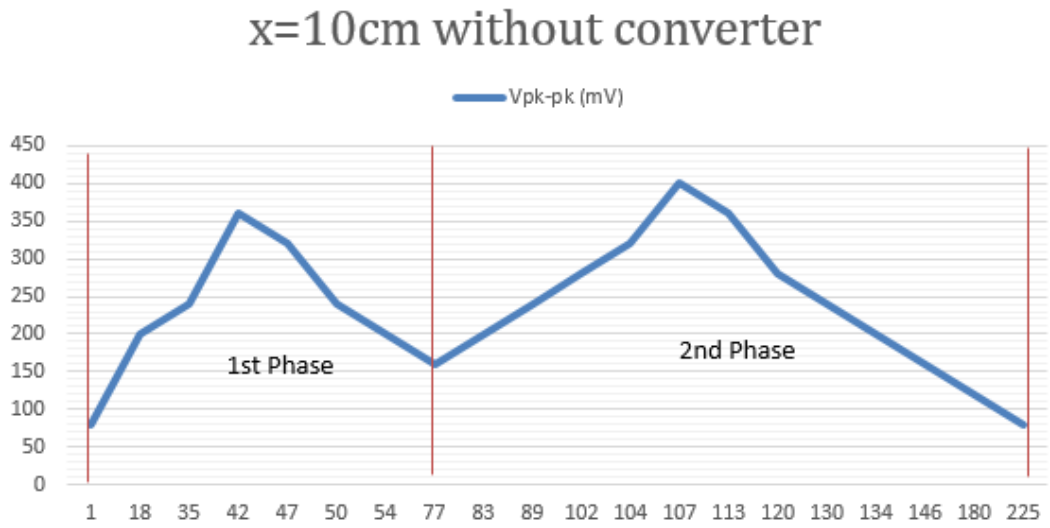

Figure.8. Output findings from sketch design of Conventional Geophone SM-24 for distance 10 cm without the step down buck converter

x=10cm	Frequency																			
Vpk-pk (mV)	1	18	35	42	47	50	54	77	83	89	102	104	107	113	120	130	134	146	180	225
Findings	80	200	240	360	320	240	200	160	200	240	280	320	400	360	280	240	200	160	120	80

Table.2. Output findings from sketch design of Conventional Geophone SM-24 for distance 10 cm without the step down buck converter

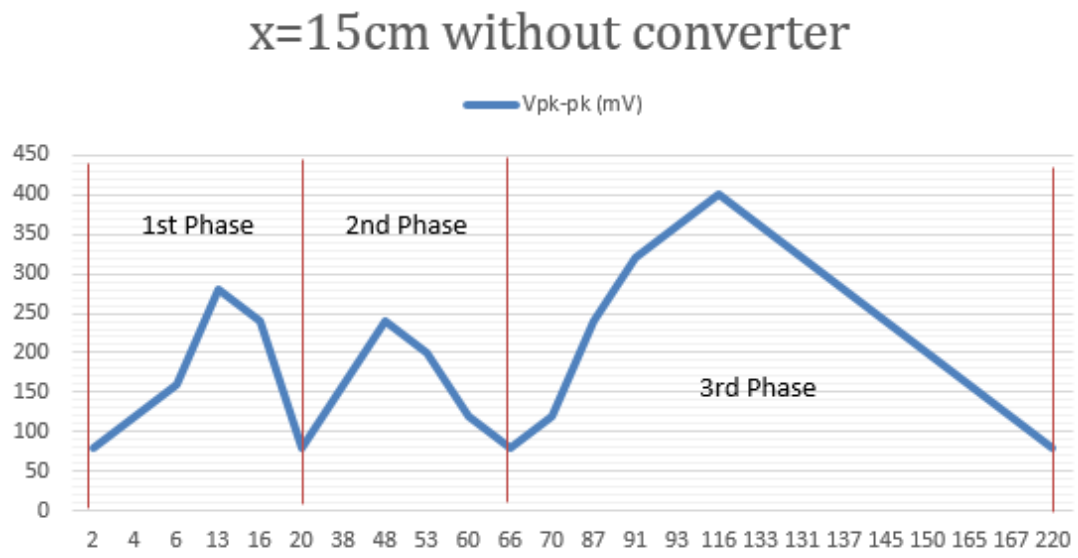

Figure.9. Output findings from sketch design of Conventional Geophone SM-24 for distance 15 cm without the step down buck converter

x=15cm	Frequency																							
Vpk-pk (mV)	2	4	6	13	16	20	38	48	53	60	66	70	87	91	93	116	133	131	137	145	150	165	167	220
Findings	80	120	160	280	240	80	160	240	200	120	80	120	240	320	360	400	360	320	280	240	200	160	120	80

Table.3. Output findings from sketch design of Conventional Geophone SM-24 for distance 15 cm without the step down buck converter

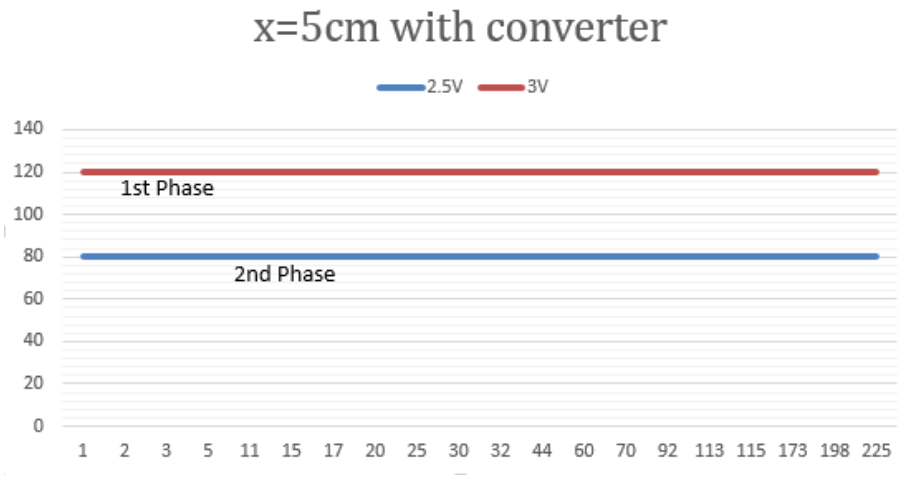

Figure.10. Output findings from sketch design of Conventional Geophone SM-24 for distance 5 cm with the step down buck converter to 2.5V and 3V output

x=5cm	Step	Frequency																			
Vpk-pk (mV)	down Converter	1	2	3	5	11	15	17	20	25	30	32	44	60	70	92	113	115	173	198	225
Findings	2.5V	80	80	80	80	80	80	80	80	80	80	80	80	80	80	80	80	80	80	80	80
	3V	120	120	120	120	120	120	120	120	120	120	120	120	120	120	120	120	120	120	120	120

Table.4. Output findings from sketch design of Conventional Geophone SM-24 for distance 5 cm with the step down buck converter to 2.5V and 3V output

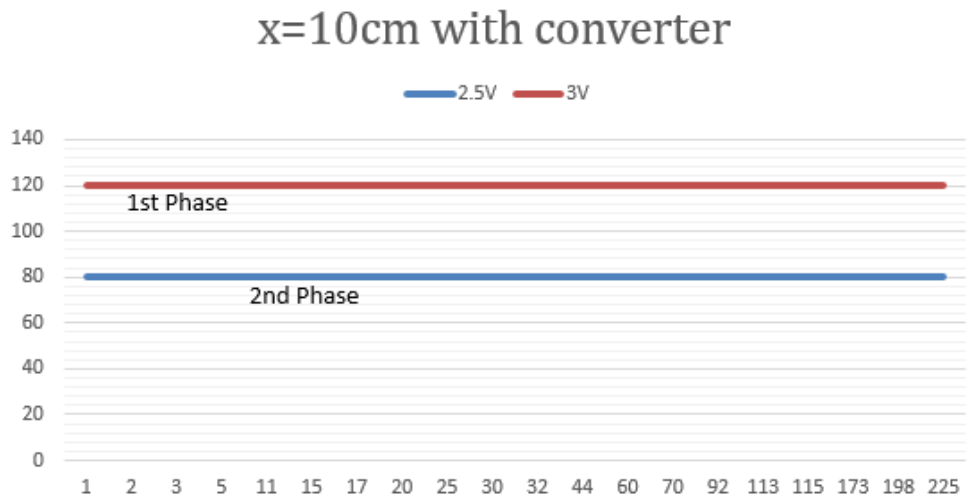

Figure.11. Output findings from sketch design of Conventional Geophone SM-24 for distance 10 cm with the step down buck converter to 2.5V and 3V output

x=10cm	Step	Frequency																			
Vpk-pk (mV)	down Converter	1	2	3	5	11	15	17	20	25	30	32	44	60	70	92	113	115	173	198	225
Findings	2.5V	80	80	80	80	80	80	80	80	80	80	80	80	80	80	80	80	80	80	80	80
	3V	120	120	120	120	120	120	120	120	120	120	120	120	120	120	120	120	120	120	120	120

Table.5. Output findings from sketch design of Conventional Geophone SM-24 for distance 10 cm with the step down buck converter to 2.5V and 3V output

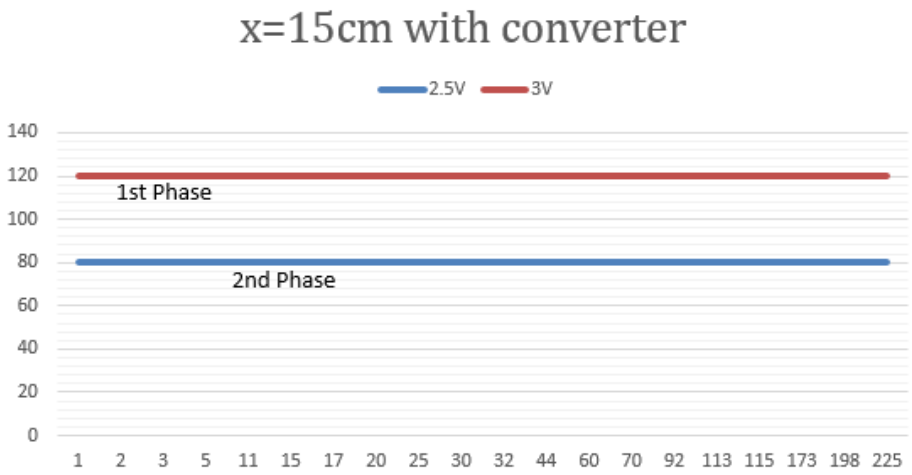

Figure.12. Output findings from sketch design of Conventional Geophone SM-24 for distance 15 cm with the step down buck converter to 2.5V and 3V output

x=10cm	Step	Frequency																			
Vpk-pk (mV)	down Converter	1	2	3	5	11	15	17	20	25	30	32	44	60	70	92	113	115	173	198	225
Findings	2.5V	80	80	80	80	80	80	80	80	80	80	80	80	80	80	80	80	80	80	80	80
	3V	120	120	120	120	120	120	120	120	120	120	120	120	120	120	120	120	120	120	120	120

Table.6. Output findings from sketch design of Conventional Geophone SM-24 for distance 15 cm with the step down buck converter to 2.5V and 3V output

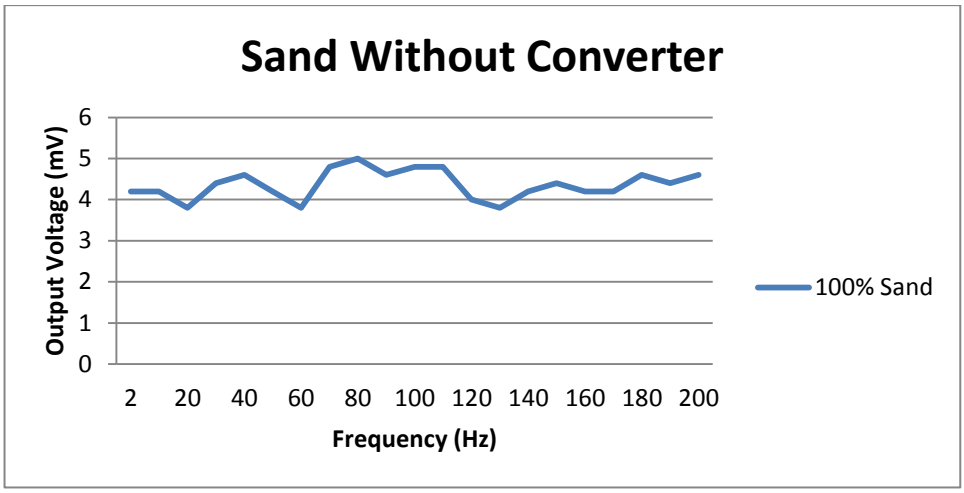

Figure.13. Output findings from sketch design of Conventional Geophone SM-24 for medium sand 100% without the converter

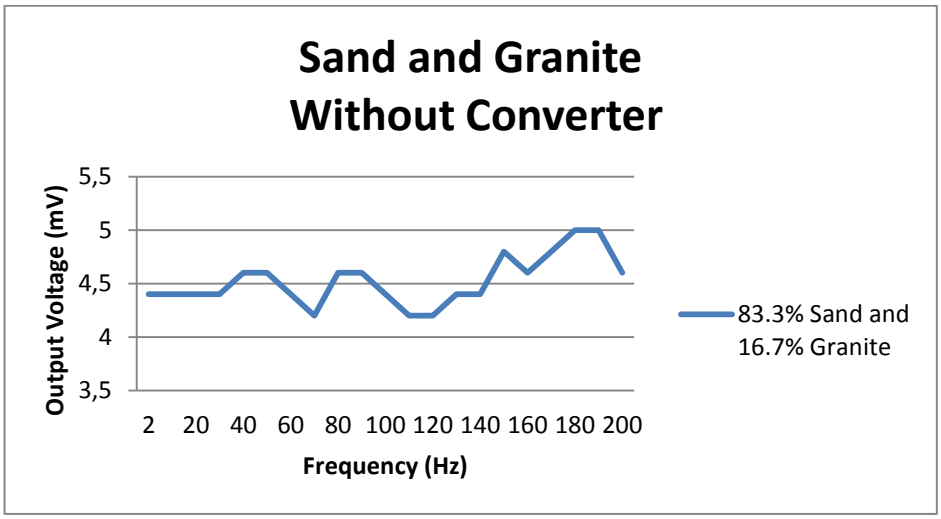

Figure.14. Output findings from sketch design of Conventional Geophone SM-24 for medium sand 83.3% and granite 16.7% without the converter

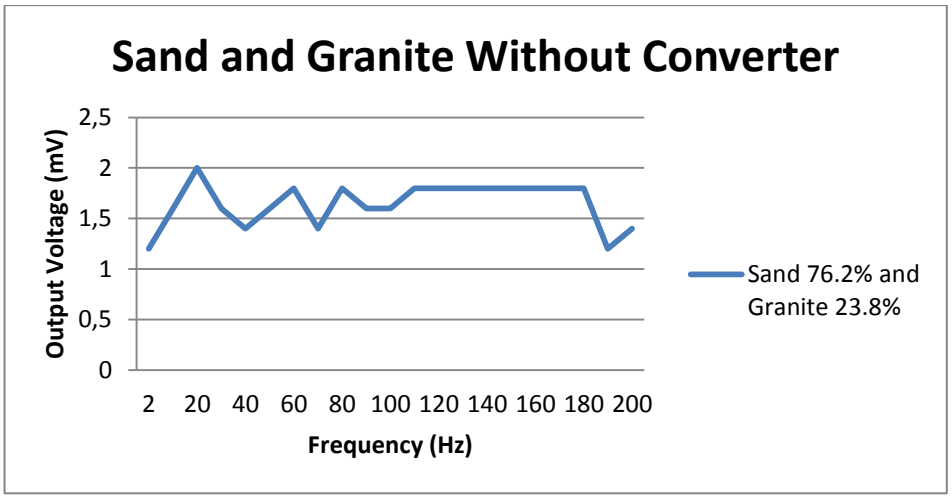

Figure.15. Output findings from sketch design of Conventional Geophone SM-24 for medium sand 76.2% and granite 23.8% without the converter

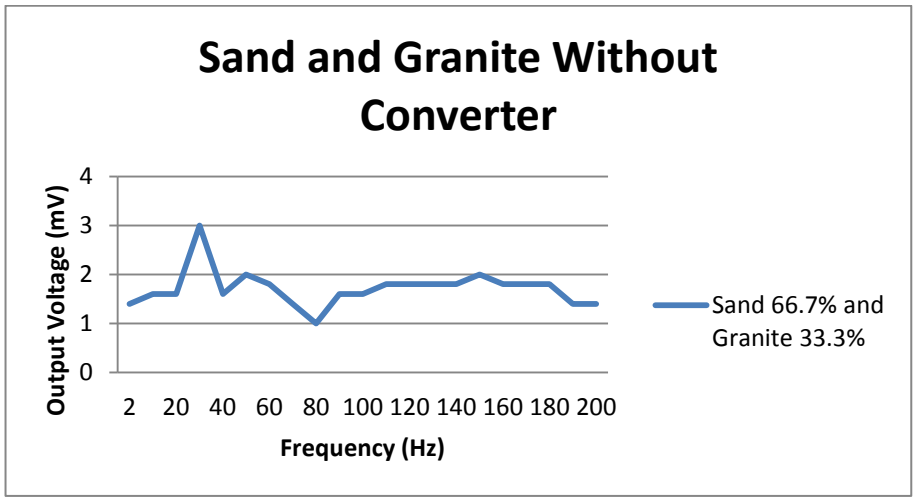

Figure.16. Output findings from sketch design of Conventional Geophone SM-24 for medium sand 66.7% and Granite 33.3% without the converter

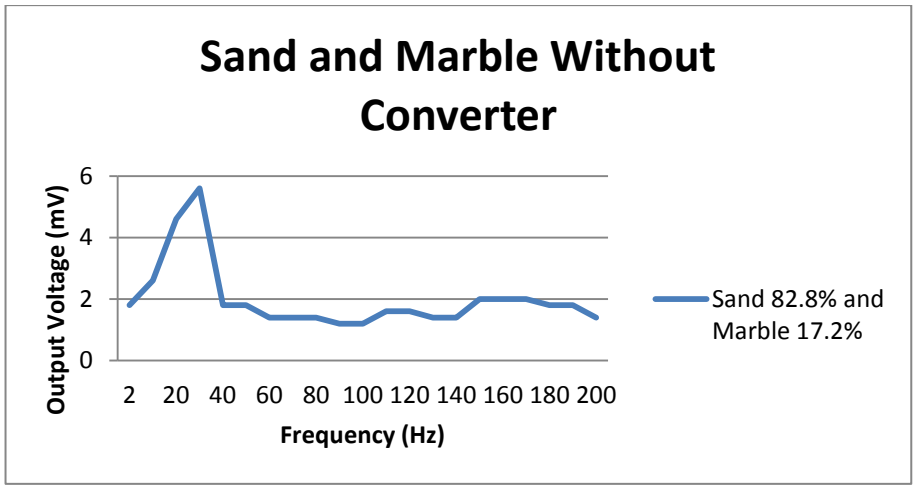

Figure.17. Output findings from sketch design of Conventional Geophone SM-24 for medium sand 82.8% and marble 17.2% without the converter

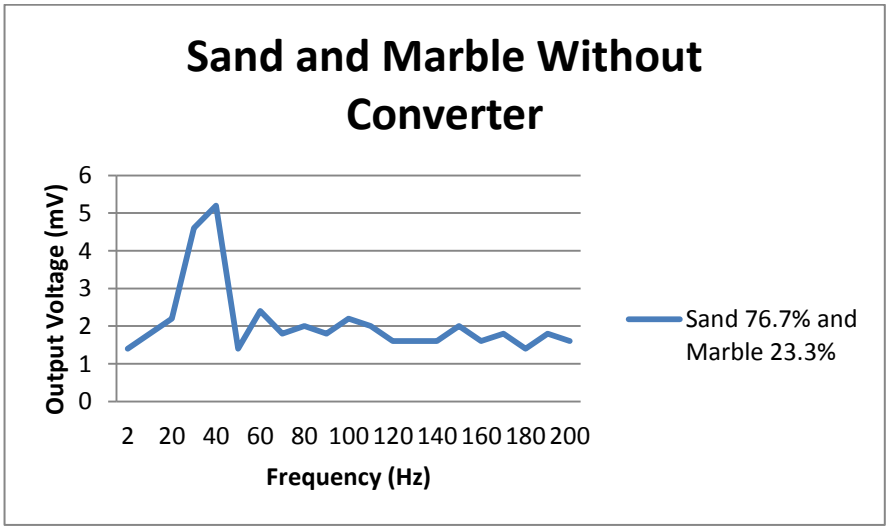

Figure.18. Output findings from sketch design of Conventional Geophone SM-24 for medium sand 76.7% and marble 23.3% without the converter

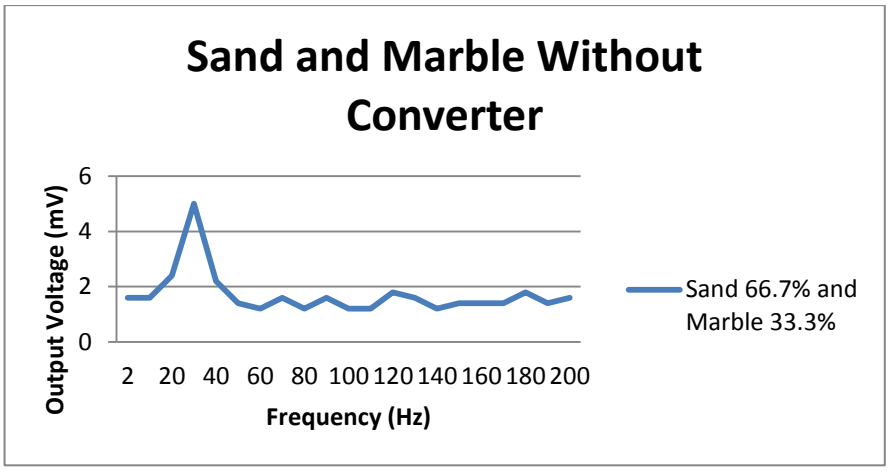

Figure.19. Output findings from sketch design of Conventional Geophone SM-24 for medium sand 66.7% and marble 33.3% without the converter

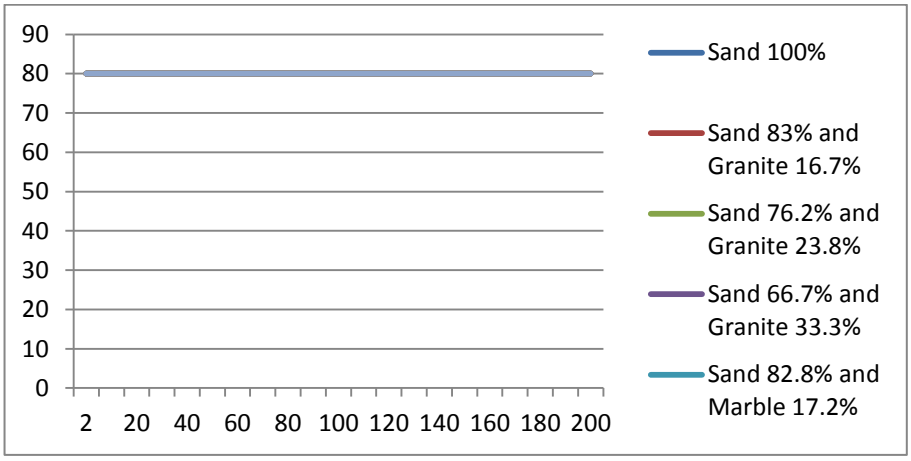

Figure.20. Output findings from sketch design of Conventional Geophone SM-24 for medium sand, granite and marble composition with the converter step down to 2,5 volts and 3 volts

4.2.3 Soil Reference Result

- ✓ Moisture Testing

Location: Seri Bota, Ipoh **Soil Description: Sample No 01**

Specimen Reference				
Container No:		**1**	**2**	**3**
Mass of wet soil + container (m_2)	**(g)**	30.0+20.70	30.10+21.00	30.00+21.20
Mass of dry soil + container (m_3)	**(g)**	46.80	46.30	43.00
Mass of container (m_1)	**(g)**	20.70	21.00	21.20
Mass of moisture (m_2- m_3)	**(g)**	3.90	4.80	8.20
Mass of dry soil (m_3- m_1)	**(g)**	26.1	25.3	21.80
Moisture Content; $\mathbf{W = \frac{(m2-m3)}{(m3-m1)} x 100\%}$ **Mean: 23.8432 %**	**(%)**	14.9425%	18.9723%	37.6147%

Table.7. Moisture testing for soil reference

***Note:** M_1 = Mass of Container M_2 = Mass of Container and wet soil M_3 = Mass of Container and dry soil

✓ Particle Size Distribution

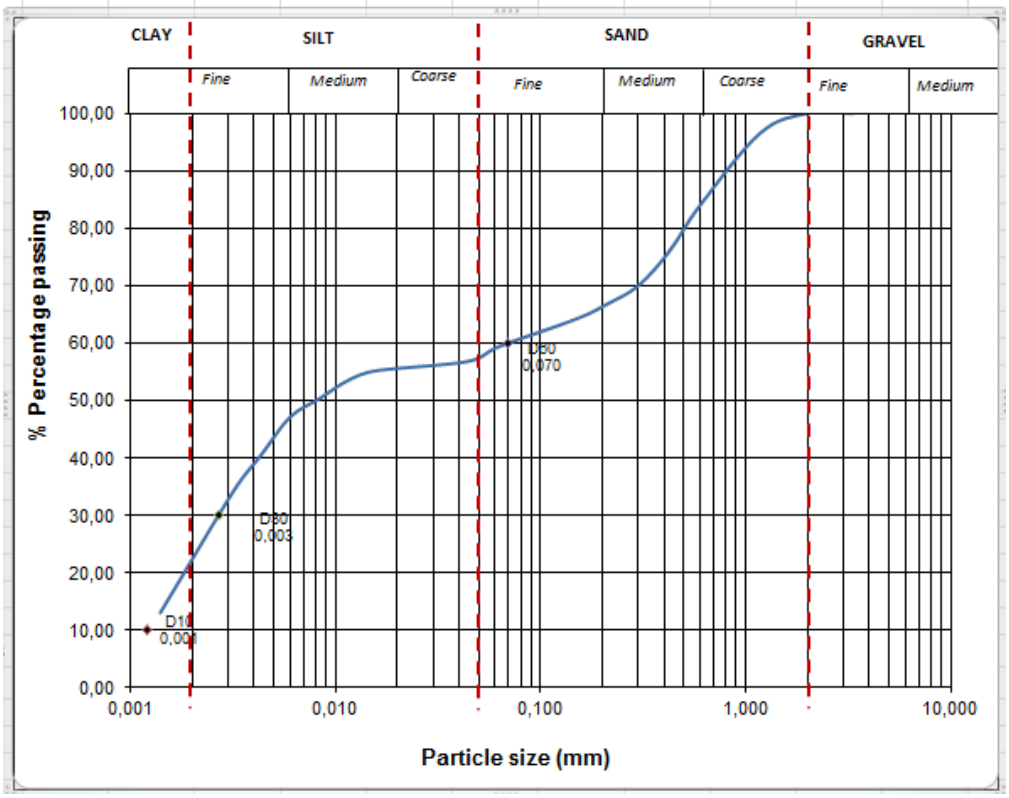

Figure.21. Particle Size Distribution testing for soil reference

✓ Shearing Box Testing

Test Summary			
Reference	A	A	A
Applied Normal Stress	5.9 kPa	0.0 kPa	17.7 kPa
Peak Strength	52.8 kPa	52.8 kPa	66.0 kPa
Corresponding Horizontal Displacement	0.419 mm	0.421 mm	0.102 mm
Residual Shear Stress			
Rate(s) of Shear Displacement	Stage 1: 0.0286mm/min	Stage 1: 0.0286mm/min	Stage 1: 0.0286mm/min
Final Height	-0.18 mm	-0.34 mm	-0.53 mm

Cumulative Displacement	0.666 mm	1.466 mm	0.722 mm
Number of Traverses	1	1	1

Table.8. Shearing Box with three times tested for soil reference

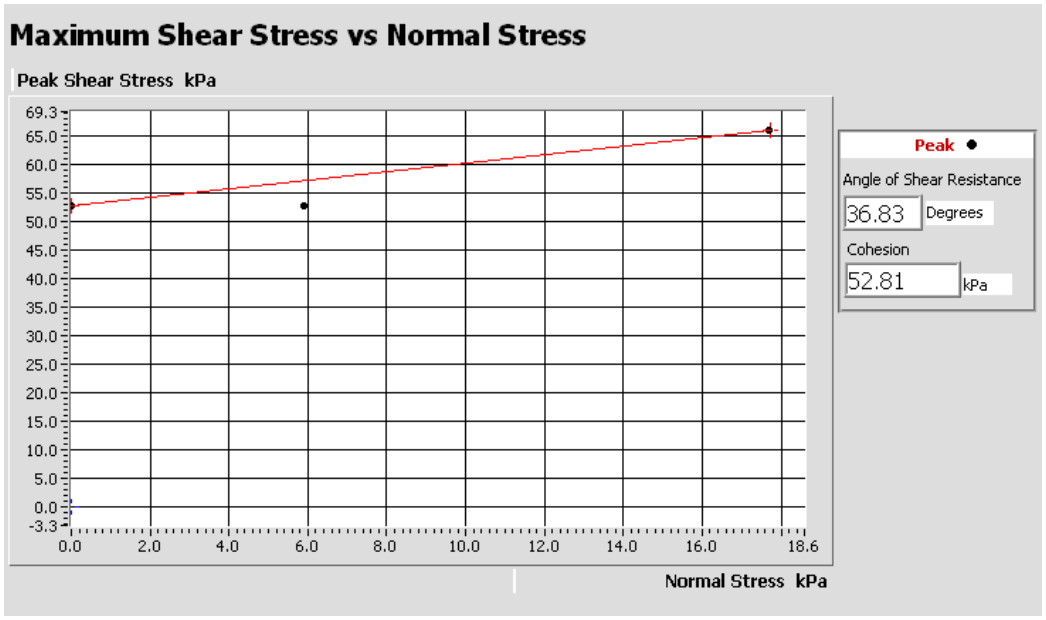

Figure.22. comparison of shear stress vs normal stress for soil reference

4.3 DISCUSSION

According to the findings on figure 7, the single element of geophone has been conducted with varies frequency from the function generator within the range of 1 Hz to 225 Hz with 5cm distance from the source vibration. The finding shown that the single element of geophone have four cycle of rise and fall period due to the set point change from each frequency which carried different behavior into the element of geophone. The lowest frequency response from the source aggressively oscillated the element into the higher voltage at each cycle period. However, the element reached the steady state after the source greater than 200 Hz.

Differently with the findings on figure 8, the single element of geophone has a sharp incremental response within two cycle of period for the range of source frequency 1 Hz to 225 Hz. In this finding, the element response affected by the extended distance of 10 cm compare with figure 7. Hence, the source wave signal from source vibration has been interfered to transmit into the element due to the distance extended.

However, when the distance has been extended into 15 cm as shown in figure 9, the element has respond the source wave differently, the period of 1 Hz to 255 Hz produced three cycle response signal for rise and fall as shown in figure 9. The element has incrementally response the source wave in the higher frequency compared with the lower frequency.

Based on figure 10, 11, and 12, the response for single element of geophone shown constant response in the output voltage compared with the response of element without converter. Additionally, the element has respond the higher output of voltage for given higher voltage has been converted.

Even though so, the element respond almost in the steady state wave form when the medium of conducted is pure sand displayed in figure 13, 14, 15, 16, 17, 18, and 19. However, if the medium was combined with rock property, such as granite and marble, it affected the output voltage respond became slightly decreased within the range of 2 Hz to 200 Hz. As the proportion of the rock increased and the proposition of the sand decreased, the output of voltage that has produced by the element became less value output. This case happened prior to the effect of the rock property which interfere the source wave to travel and transmit the signal wave through the receiver of the element.

However, the finding in the single element of geophone using properties of sand and rock has displayed constant output voltage in the figure 20. The element has been responding the constant value for any change within the range of 2 Hz to 200 Hz. Even though so, the advanced experiment might be recommended to seek the actual response of the single element of geophone.

CHAPTER 5
CONCLUSION AND RECOMMENDATION

5.1 CONCLUSION

In a conclusion, this project has been completed the first stage of conceptual studies which are involved understanding about basic exploration and vertical seismic profiling method used for land seismic survey method. Furthermore, the project has been implemented the project development for performed soil testing method, single plate design, single element of geophones SM-24 implementation without converter within distance 5cm, 10cm, and 15cm, performed single element of geophones SM-24 implementation without converter within distance 5cm, 10cm, and 15cm and lastly combined the testing of single element of geophone in the different of medium proportion such as sand and rock (granite and marble).

The result shown that the single element of conventional geophone SM-24 implemented without converter has a significant effect of output voltage whenever the frequency increased in one cycle 1Hz – 225Hz. In distance 5cm, the output voltage reacted in rise and fall response in every frequency steps (Hz) changed. Therefore, the output voltage from figure.7 have a rise and fall line. In this distance, the steady state output voltage have a wider range in the first phase of one cycle frequency.

Different with distance 5cm, in the actual measurement for distance 10cm and 15cm the result shown that the steady stead output voltage have a wider range in the second phase and third phase of one cycle frequency. Even though, the graph remained to have a rise and fall response through the frequency changed.

However, for the actual measurement of single element geophones SM-24 added using converter within distance 5cm, 10cm, and 15cm has no defect into the output voltage, it respond same with figure 20 that element tested by medium sand and rock. The difference shown solitary by having different voltage step down which are comprehensive to get the higher output voltage. Otherwise, the output voltage in the frequency changed are remained the same.

Moreover, the element respond, almost in the steady state wave form when the medium of conducted is pure sand displayed in figure 13, 14, 15, 16, 17, 18, and 19. However, if the medium was combined with rock property, such as granite and marble, it affected the output voltage respond became slightly decreased within the range of 2 Hz to 200 Hz. As the proportion of the rock increased and the proposition of the sand decreased, the output of voltage that has produced by the element became less value output. This case happened prior to the effect of the rock property which interfere the source wave to travel and transmit the signal wave through the receiver of the element.

5.2 RECOMMENDATION

Refers to the finding shown, the additional method to increment the value of the output voltage by having a large voltage input or change in the impedance geophone. However, the larger input voltage injected will not give a response or may get a defect to failure for the geophones to response the sensitivity. Therefore, implemented the conventional geophone using different material of windings may help into better performance or smaller dimension.

In a conclusion, this project will be continued for implemented single element of geophones SM-24 through three elements of geophones SM-24 which are implemented in the soil medium references.

REFERENCES

[1] Farfour, M., & Jung Yoon, W. A review on multicomponent seismology: a potential seismic application for reservoir characterization: South Korea: Journal of Advanced Research. 2015

[2] Laurence, R. Lines., & Rachel, T. Newrick., 2004, Fundamental of geophysical interpretation: Florida, USA: Society of Exploration Geophysicists.

[3] Iversion WP, Fahmy BA, Smithson SB. VpVs from mode – converted P – SV reflections. Geophysics 1989; 54: 843 – 52

[4] Y. Ashida. Seismic imaging ahead of a tunnel face with three component geophones. 2001. Japan

[5] Hardage, B. A., 1983, Vertical seismic profiling – Part A: Principles: Geophysical Press Limited.

[6] Sattel G, Frey P, Amberg R. Prediction ahead of the tunnel face by seismic methods, pilot project in Centovailli Tunnel, Locarno, Switzerland. First Break 1992; 10: 19 – 25.

[7] Nejati, M., & Hashemi, H, 2012, Migrated Exploding Reflectors in Evaluation of Finite Difference Solution for Inhomogeneous Seismic Model.

[8] Geometrics, crosshole seismic testing, retrieved: 16 February 2016, 00:07 am, http://www.geometrics.com/applications/geophysical-methods/crosshole-seismic-testing/

[9] S, L, Shah., 2000, Seismic data acquisition and recording, New Delhi: Allied Publisher Ltd.

[10] Ashida Y, Hirano T, Inaba T. Looking ahead of tunnel face by use of equi – travel time planes. Proceeding of International Workshop: Application of Geophysics to Rock Engineering 1997, p 83 – 84.

[11] Andreas, Stark., 2010, Seismic method & applications: Florida, USA: BrownWalker Press.

APPENDIX

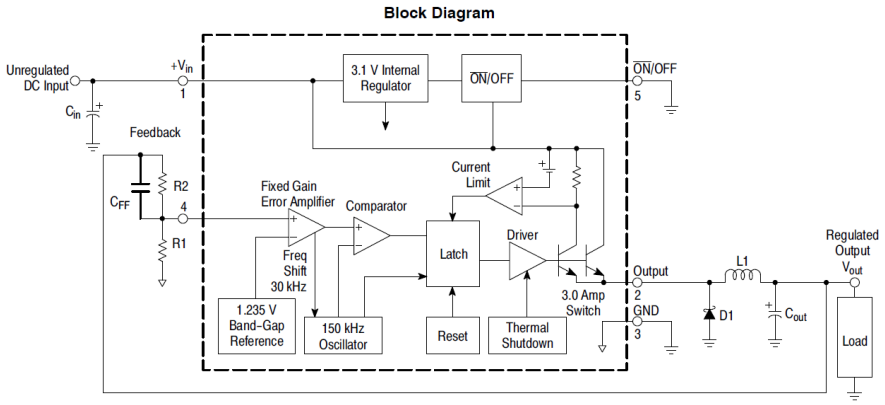

Figure.23. Step down buck converter datasheet

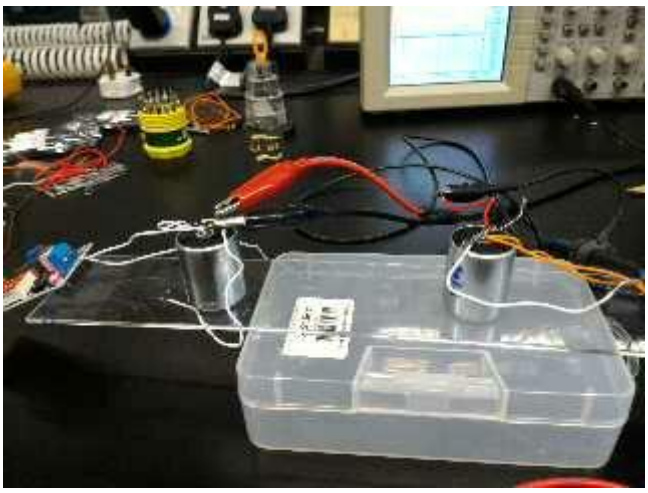

Figure.24. Application Single Component Transducer using Single Plate

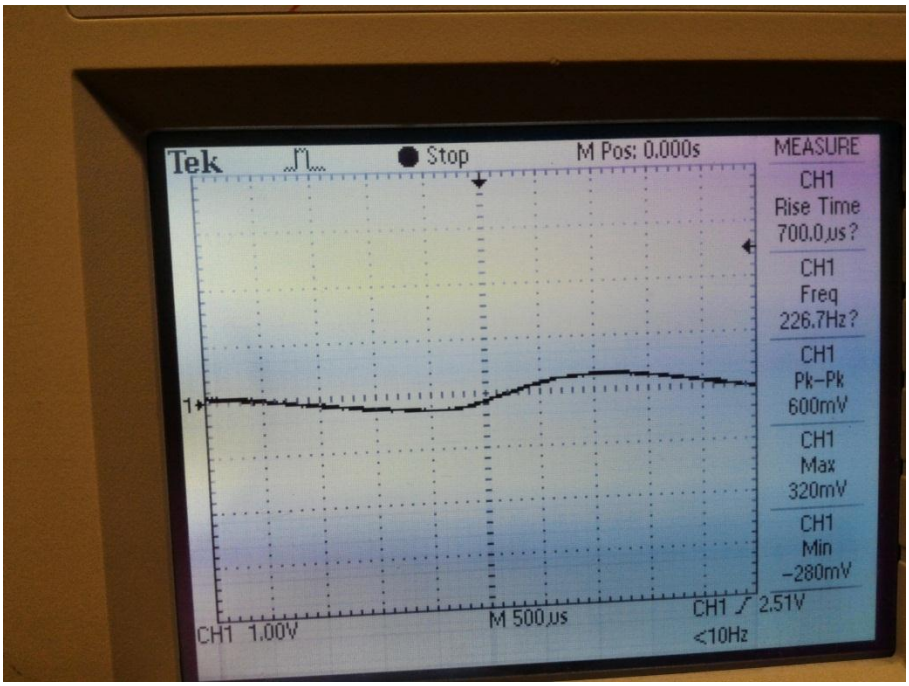

Figure.25. Finding of Single Component Transducer using Single Plate at 120 Hz without Converter

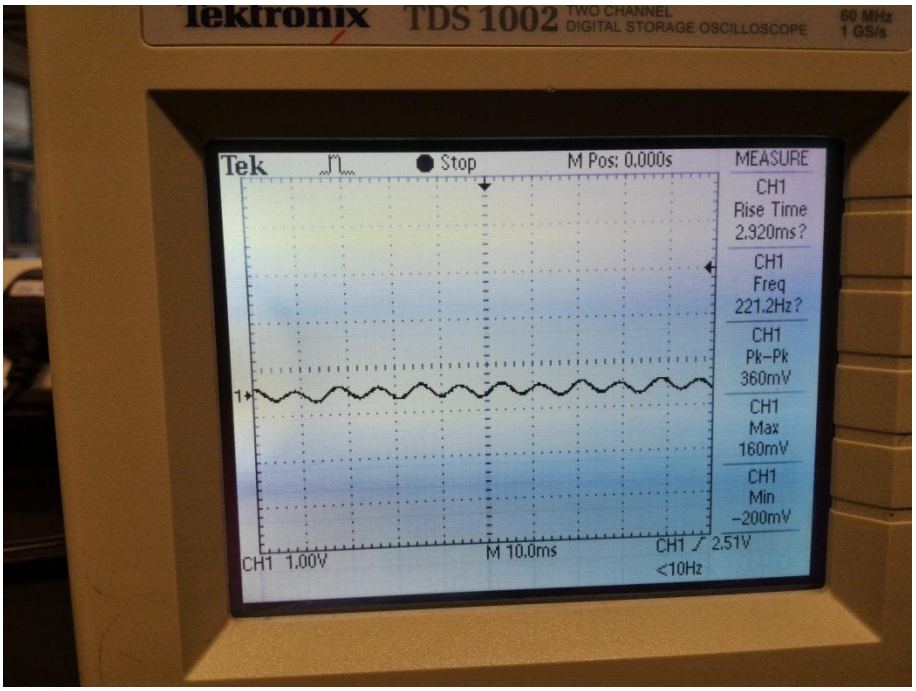

Figure.26. Finding of Single Component Transducer using Single Plate at 110 Hz with Converter

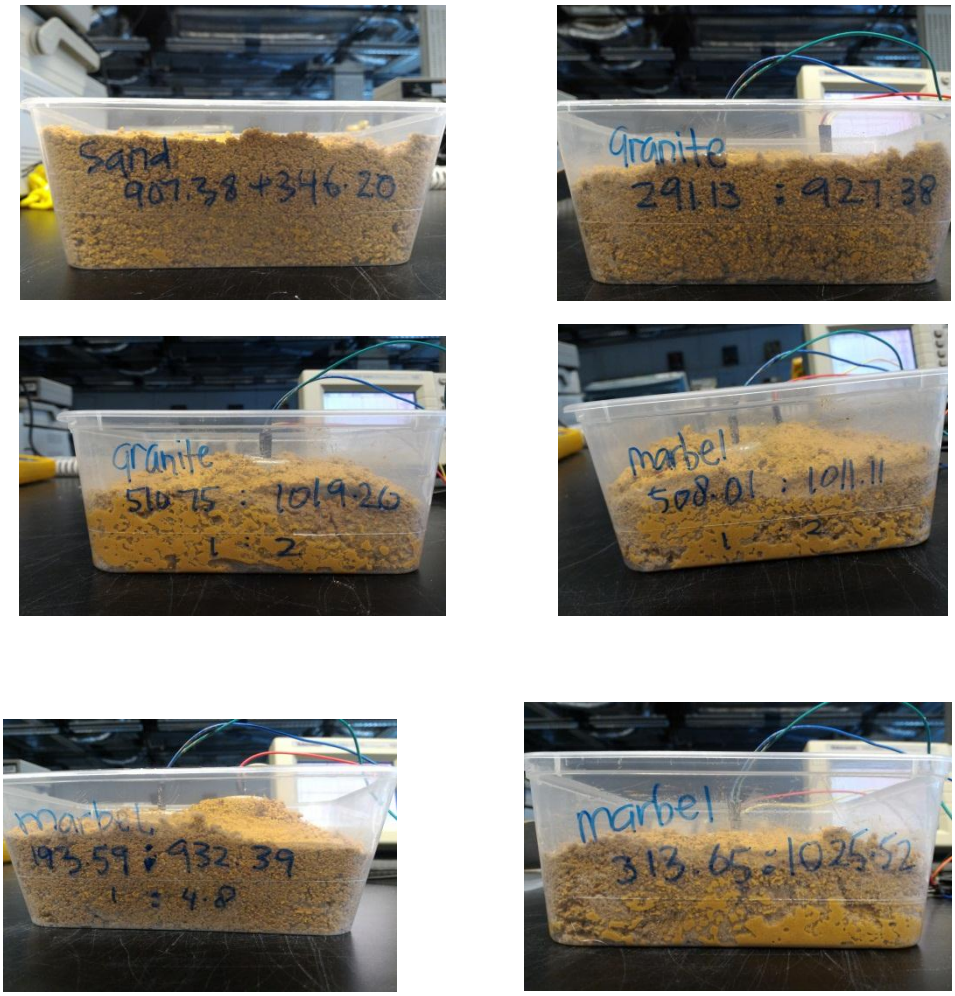

Figure.27. Material Soil and Rock Sample

Journal's Title, Vo34l. x, 20xx, no. xx, xxx - xxx
HIKARI Ltd, www.m-hikari.com
http://dx.doi.org/10.12988/

Seismic Boundary Reflection Approximation

By Autoregression

Umairia Malik1

Department of Fundamental and Applied Sciences
Universiti Teknologi PETRONAS
Bandar Seri Iskandar 31750 Tronoh Perak- Malaysia
umairiamalik89@gmail.com

Dennis Ling Chuan Ching2

Department of Fundamental and Applied Sciences
Universiti Teknologi PETRONAS
Bandar Seri Iskandar 31750 Tronoh Perak- Malaysia
dennis.ling@petronas.com.my

Hanita Daud3

Department of Fundamental and Applied Sciences
Universiti Teknologi PETRONAS
Bandar Seri Iskandar 31750 Tronoh Perak- Malaysia
hanita_daud@petronas.com.my

Vikri Januarisma4

Department of Electrical and Electronics Engineering
Universiti Teknologi PETRONAS
Bandar Seri Iskandar 31750 Tronoh Perak- Malaysia
vikrijanuarisma@gmail.com

Abstract

Seismic waves are used for the detection of reservoirs and material boundaries in presence of fracture. Finite difference method (FDM) model the elastic waves in homogenous medium. The physical boundary is set to rigid boundary condition while the computational boundaries are computed on Clayton Engquist (CE) boundary condition. After getting the synthetic gathers, a preprocessing step i.e. automatic gain control (AGC) is used to rise the subsurface reflections. Then autoregressive of order one is employed to model the subsurface reflections. The estimated autoregressive model for synthetic data explains the 94.739% variability and amplitude value of $-5.5798e^{-09}$ similar to real data $-1.09173e^{-09}$ when all the values in predictor are zero. The comparison with real model provides evidence that predicted model can interpret the acquisition geometry material properties and its boundary in the real subsurface.

Keywords: Finite difference method, Clayton Engquist, Rigid boundary, Automatic gain control

1 Introduction

The accurate simulations of wave phenomenon in bounded and unbounded mediums are an imperative in physical areas such as seismology, elasticity, acoustics, and electromagnetism. The simulation of waves consists of a physical system of partial differential equations that depicts the underlying physics. Wave propagation is categorized based on their mediums such as elastic waves can pass through solids, acoustic equations are for fluid mediums, and Maxwell's equations model the electromagnetic waves [1].

Seismic forward modeling is a procedure to simulate the waves in the Earth's subsurface. This procedure is composed of two main categories, namely, geological model building, and numerical computation seismic response for the model. The forward process explains the wave propagation from the source to the distribution in the subsurface and back to receivers [2]. The synthetic seismic data are generated based on the particular geological model and thereafter compared with real data. The concurrence of acceptable accuracy between the

synthetic and real data demonstrates that the assumed geological model as an accurate subsurface model. In another case, if the geological model provides the sufficient accuracy, the synthetic data confirm the selection of acquisition geometry, processing parameters, and assist in interpretation [3]. While seismic modeling methods are classified into three categories; ray tracing methods, integral equation methods, and direct methods. In ray tracing methods or asymptotic methods, the wave fields are characterized by travel time and associated amplitude. The integral equation methods, seismic wave field is presented through the integral equations. The direct methods come up with the numerical solution of wave equations. Finite difference method also named as grid methods, discretize the model into a finite number of points. These methods are capable of modeling the seismic waves in heterogeneous medium accurately [4].

There are three different formulations for the Earth model; acoustic, elastic isotropic and anisotropic models respectively. An isotropic elastic model is portrayed through the compressional velocity denoted as VP, shear velocity (VS) and density ρ. The isotropic elastic models consist of compressional and shear wave fields. The particle motion in compressional wavefield is normal to the direction of propagation; in contrast of compressional wavefield, tangential particle motion to the propagated direction refers the shear waves and has lower velocity than the compressional waves. In the time of propagation these conversed particle motions interact with each other [5].

Finite difference method is employed for modeling the 2D P-SV wave propagation in the homogeneous medium on staggered grid scheme. This method is practiced in both time and space and the selection of nodal points depends on the grid scheme. There are two major categories of grid schemes. Staggered and non-staggered grid schemes. The definitive work on non-staggered in 1986 was done by Alterman and Karal and by Kelly, Ward, Treitel, and Alford in 1976. Jean Virieux started the work on SH wave modeling by using the velocity-stress system on a discrete grid. Later he extended his work on P-SV wave modeling in the heterogeneous medium by using the staggered grid scheme and describes the non-existence of two velocity components at same node for completion of staggered grid [6].

There is a distinction between physical boundaries and computational boundaries of a subsurface model. In a subsurface model rock-rock, rock-water, water-air, rock-air and the top free surface of the model are called the physical boundaries, while, bottom boundary and the two sides of the subsurface model; left and right sides are named as computational boundaries. A comparative study of the free surface boundary condition is taken by [7]. For solving the problem of computational boundaries there is, Clayton Engquist (CE) boundary condition and a non-reflecting boundary condition that Cerjan et al. proposed in 1985 [6]. There are some other boundary conditions are like Perfectly Matched Layer (PML) condition, exact boundary condition, and a new absorbing boundary condition as mentioned by [8].

The finite difference method estimates the wavefield at a node from the wave field's values of the same node and surrounded nodes at a previous node then there is no issue in solving the computational boundaries. The computational boundaries behave like the physical boundaries when the wave fields are set to zero on computational boundaries called the rigid boundary condition. In rigid boundary condition all the incidental seismic energy reflected back to sensors. Rigid boundary condition gives very strong boundary reflection because it doesn't generate any motion of the boundary. Thus, the reflections are named as artificial reflections [6].

The limitation on available computational source give rise the computational and physical boundary problem in finite difference method and has been a continuous issue in wave modeling. This study is concerned about modeling artificial subsurface reflections for the rigid boundary by using the time series autoregressive model. Then, a comparison of real and synthetic data is employed to study the material boundary in real data. Through modeling the subsurface reflection will assist in estimating the materials without employing any long processing of exploration seismology.

2 Elastic Wave Equations and Rigid Boundary Condition

In order to facilitate the treatment of rigid boundary condition presented here, we consider the top surface of a rectangular interfaced subsurface model as rigid boundary condition where particle displacements or velocities are set to zero [6]. The 2D elastic wave equations in isotropic homogeneous medium for a velocity-stress system are as follows:

$$\rho(x,z)\frac{\partial v_1}{\partial t} = \frac{\partial \tau_{11}}{\partial x_1} + \frac{\partial \tau_{13}}{\partial x_3} \tag{1}$$

$$\rho(x,z)\frac{\partial v_3}{\partial t} = \frac{\partial \tau_{13}}{\partial x_1} + \frac{\partial \tau_{33}}{\partial x_3} \tag{2}$$

$$\frac{\partial \tau_{11}}{\partial t} = (\lambda + 2\mu)\frac{\partial v_1}{\partial x_1} + \lambda\frac{\partial v_3}{\partial x_3} \tag{3}$$

$$\frac{\partial \tau_{33}}{\partial t} = (\lambda + 2\mu)\frac{\partial v_3}{\partial x_3} + \lambda\frac{\partial v_1}{\partial x_1} \tag{4}$$

$$\frac{\partial \tau_{13}}{\partial t} = \mu\left(\frac{\partial v_1}{\partial x_3} + \frac{\partial v_3}{\partial x_1}\right) \tag{5}$$

where, λ and μ are Lamé parameter and $\rho(x,z)$ is density. v_1, and v_3 are horizontal and vertical particle velocities in x and z directions, respectively. τ_{11}, τ_{33} and τ_{13} are stress tensors in x, z and xz direction. In Cartesian coordinate system, a set of grid points is defined as x_i, z_j, t_k for a 2D model. Where, $x_i = x_o + i\delta_x$, $z_j = z_o + j\delta_z$, $t_k = t_o + k\Delta t$, and $i, j, k = 0,1,2,\ldots$. Generally the grid spacing in x and z directions are same i.e. $\delta_x = \delta_z = \delta$. The accuracy of finite difference method depends on the δ. Δt is the time step. The Nyquist sampling criteria helps to select the number of time steps in finite difference modeling as mention in equation (6).

$$\Delta t \leq \frac{\sqrt{2}}{\pi}\frac{\delta_x}{V_{max}} \tag{6}$$

where, V_{max} is the maximum velocity in the model [9].

As the finite difference approximations of the above equations (1) to (5) are taken on a staggered grid scheme and mention from equation (7) to (11). Thus, the discretization is described through the following figure.

In Figure 1 ◇ = τ_{11}, τ_{33}, ◯ = τ_{13}, ◆ = v_3 and ● = v_1 and ⊗ = fictitious boundary.

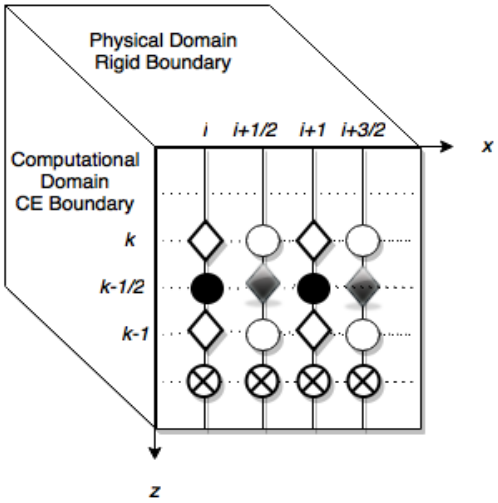

Figure 1. Discretization and Rigid Boundary Condition

$$\rho\left(\frac{{v_1}_{i,k}^{n+\frac{1}{2}}-{v_1}_{i,k}^{n-\frac{1}{2}}}{\Delta t}\right)=\left\{\left(\frac{{\tau_{11}}_{i+\frac{1}{2},k}^{n}-{\tau_{11}}_{i-\frac{1}{2},k}^{n}}{h}\right)+\left(\frac{{\tau_{13}}_{i,k+\frac{1}{2}}^{n}-{\tau_{13}}_{i,k-\frac{1}{2}}^{n}}{h}\right)\right\} \tag{7}$$

$$\rho\left(\frac{{v_3}_{i+\frac{1}{2},k+\frac{1}{2}}^{n+\frac{1}{2}}-{v_3}_{i+\frac{1}{2},k+\frac{1}{2}}^{n-\frac{1}{2}}}{\Delta t}\right)=\left\{\left(\frac{{\tau_{13}}_{i+1,k+\frac{1}{2}}^{n}-{\tau_{13}}_{i,k+\frac{1}{2}}^{n}}{h}\right)+\left(\frac{{\tau_{33}}_{i+\frac{1}{2},k+1}^{n}-{\tau_{33}}_{i+\frac{1}{2},k}^{n}}{h}\right)\right\} \tag{8}$$

$$\left(\frac{{\tau_{11}}_{i+\frac{1}{2},k}^{n+1}-{\tau_{11}}_{i+\frac{1}{2},k}^{n}}{\Delta t}\right)=(\lambda+2\mu)_{i+\frac{1}{2},k}\left(\frac{{v_1}_{i+1,k}^{n+\frac{1}{2}}-{v_1}_{i,k}^{n+\frac{1}{2}}}{h}\right)+\lambda_{i+\frac{1}{2},k}\left(\frac{{\tau_{33}}_{i+\frac{1}{2},k+\frac{1}{2}}^{n+\frac{1}{2}}-{\tau_{33}}_{i+\frac{1}{2},k-\frac{1}{2}}^{n+\frac{1}{2}}}{h}\right) \tag{9}$$

$$\left(\frac{{\tau_{i+\frac{1}{2},k}}^{n+1}-{\tau_{33}}_{i+\frac{1}{2},k}^{n}}{\Delta t}\right)=(\lambda+2\mu)_{i+\frac{1}{2},k}\left(\frac{{\tau_{33}}_{i+\frac{1}{2},k+\frac{1}{2}}^{n+\frac{1}{2}}-{\tau_{33}}_{i+\frac{1}{2},k-\frac{1}{2}}^{n+\frac{1}{2}}}{h}\right)+\lambda_{i+\frac{1}{2},k}\left(\frac{{v_1}_{i+1,k}^{n+\frac{1}{2}}-{v_1}_{i,k}^{n+\frac{1}{2}}}{h}\right) \tag{10}$$

$$\left(\frac{{\tau_{13}}_{i,k+\frac{1}{2}}^{n+1}-{\tau_{13}}_{i,k+\frac{1}{2}}^{n}}{\Delta t}\right)=\mu_{i,k+\frac{1}{2}}\left(\frac{{v_3}_{i+\frac{1}{2},k+\frac{1}{2}}^{n+\frac{1}{2}}-{v_3}_{i-\frac{1}{2},k+\frac{1}{2}}^{n+\frac{1}{2}}}{h}+\frac{{v_1}_{i+1,k}^{n+\frac{1}{2}}-{v_1}_{i,k}^{n+\frac{1}{2}}}{h}\right) \quad (11)$$

In order to completely model the seismic wave propagation, it is essential to specify the initial and boundary conditions. The stress and particle displacement or velocity and their time derivatives are zero before the seismic source is fired [10]

$$v_i=\frac{\partial U}{\partial t}=0 \qquad t\le 0, \quad i=1,2 \quad (12)$$

$$\tau_{ij}=\frac{\partial \tau_{ij}}{\partial t}=0 \qquad t\le 0, \quad i,j=1,2 \quad (13)$$

where, v_i is the particle velocity and τ_{ij} is stress tensor. Figure 1 also illustrate the rigid boundary condition. In which the line *k-1/2* is considered as rigid boundary and all particle and vertical velocities are set to zero though, there is no real numerical nodes on this line. The left, right and bottom boundaries are set to Clayton Engquist (CE) boundary condition. The equations (14) and (15) are CE conditions.

$$\frac{\partial v_1}{\partial x_1}+\frac{1}{V_S}\frac{\partial v_1}{\partial t}=0 \quad (14)$$

$$\frac{\partial v_3}{\partial x_3}+\frac{1}{V_P}\frac{\partial v_3}{\partial t}=0 \quad (15)$$

The finite difference approximation of equation (14) and (15) are given below:

$$\left(\frac{{v_1}_{i+1,k}^{n}-{v_1}_{i,k}^{n}}{h}\right)+\frac{1}{Vs}\left(\frac{{v_1}_{i,k}^{n+\frac{1}{2}}-{v_1}_{i,k}^{n-\frac{1}{2}}}{\Delta t}\right)=0 \quad (16)$$

$$\left(\frac{{v_3}_{i+\frac{1}{2},k+\frac{1}{2}}^{n+\frac{1}{2}}-{v_3}_{i+\frac{1}{2},k-\frac{1}{2}}^{n+\frac{1}{2}}}{h}\right)+\frac{1}{Vp}\left(\frac{{v_3}_{i+\frac{1}{2},k+\frac{1}{2}}^{n+\frac{1}{2}}-{v_3}_{i+\frac{1}{2},k+\frac{1}{2}}^{n-\frac{1}{2}}}{\Delta t}\right)=0 \quad (17)$$

3 Simulation

The seismic modeling plays a crucial role in exploration seismology like seismic data acquisition, processing, interpretation and reservoir characterization. The process of seismic modeling starts with building the model geometry followed by different propagating velocity and density within different units of the model. The geometry of model consists of stratigraphic horizons and faults irrespective of the modeling approach. The horizons of top and base of reservoir rock, top, and base of salt and surface that have significant variations in velocities are examples of horizons [2].

Assuming a velocity model structure *C(x,z)* is known with the length of 2000m and depth of 1000m. The near surface velocity model has a diagonal

interface and its layers has chalk and granite material properties, respectively. In the presence of chalk material in upper layer, the P wave velocity has the range of 2300 m/s to 2600 m/s, S wave velocity varies from 1100 m/s to 1300 m/s and the density is 1.8 to 3.1 g/cm^3 and the lower layer has the properties of granite which are as follows: P wave velocity varies with in the range of 4500 to 6000 m/s, the S wave velocity has range of 2500 to 3300 m/s and the density is between 2.5 to 2.7 g/cm^3 [11]. The geometry of source location S_{shot} *(x,z)*, is specified as the split spread geometry where the receivers are around the S_{shot} *(x,z)*. The S_{shot} *(x,z)* spacing is 25 m in length while there is zero spacing in depth and consequently the grid size , δ is 2.5m. There are total thirty receivers that are set on the both sides of source, S_{shot} *(x,z)*. The receiver's position is defined along one line in the computational domain as shown in Figure 2.

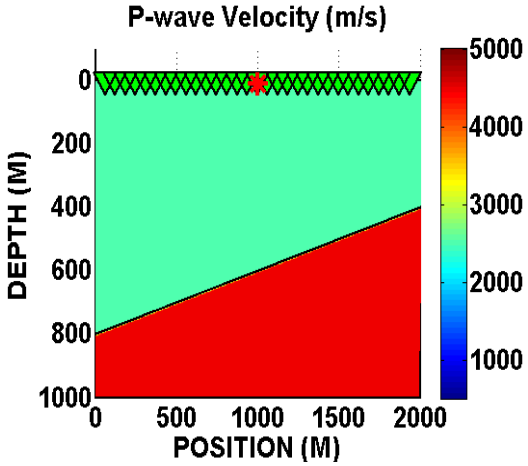

Figure 2: Velocity Model

For the collection of seismic data, It requires an energy source and sensors to receive the propagated energy from the subsurface. Dynamite and other explosive sources provide the principal energy source for seismic prospecting systems. There is no other source of energy that provides such a compact package of concentrated energy. Explosions are man-made sources with specific location and time. They are sufficient to generate the seismic waves which can be recorded from several kilometers (km) to hundreds of kilometers [12]. In this subsurface model, we use the deep explosion source of energy. This source has the property to distribute the energy in the solid medium, as well as, the four force vectors are equivalent in magnitude in all directions [13].

The seismic energy source produces the seismic pulses that make the seismic wavelet, travel through the subsurface beds or strata and carry the geological information. There are different types of wavelets like ricker wavelet, zero-phase wavelet, maximum wavelets, mixed wavelets and minimum phase wavelet. The selection of wavelet makes a noticeable difference to the appearance of synthetic

data. Focus on minimum phase wavelet, a short time duration wavelet that concentrated the energy at the start of the wavelet. This wavelet is zero before the time is zero and has a rapid buildup of energy. The actual source signature of these wavelets is nearer to the source signature of explosives or air guns. This is a preferred wavelet because in the presence of reflectors there central peak at zero times helps in interpretation [14]. The central frequency for this minimum phase wavelet is chosen to 30 Hz. The synthetic modeling is done by using the CREWES mFD2D package in Matlab.

The variation of amplitude is the key issue while interpreting the result of propagation effect from different rock layers. Usually, the traces near the surface have strong amplitudes at early times while at far-offset traces synthetic data have weak and non-existent reflections. For simply mapping the amplitude, an easy way is to apply the automatic gain control (AGC). The generated synthetic traces are equalize by using the automatic gain control in order to correct the geometrical spreading and attenuation of propagating wave fronts. Its objective is to scale the synthetic data such that in a sliding window all the traces have average root means square (RMS) and average reflectivity is invariant [15].
Automatic gain control (AGC) is a trace by trace mechanism, each trace is processed independently. A frequently used deterministic approach is called *t*-square method, the traces are multiplied with the square of two way travel [16].

$$GF = t^2 \tag{18}$$

The change in the amplitude amount depends on the selection of sliding window. Here in synthetic data a sliding window of 100 milliseconds (ms) is selected and *t*-square AGC method is employed.

After applying the AGC, the amplitude information is altered. As the near velocity model contains the reflector or interface, the gathered reflections will contain the response of it. Thus, the altered reflections are modeled through the autoregression.

4 Results and Discussion

A horizontal seismic profiling (HSP) is used in the geological model, in which the receivers and sources are placed on the surface [17]. Then a single shot is recorded as data $D_{shot}(x,t)$ and AGC is applied as a preprocessing step. In the near surface velocity model the rigid boundary condition is used on the top surface physical boundary that is set to zero velocities at particular staggered grid points and CE boundary condition is employed on other boundaries, such as left, right and bottom boundary. Figure 2 shows the synthetic data generated by using the CREWES mFD2D package. Figure 3 is the trace of real data taken from the Blackfoot field Alberta Canada. It was a big 3C-3D survey conducted in 1995 and consists of two different patches with the total area of 16.8 square kilometers [23].

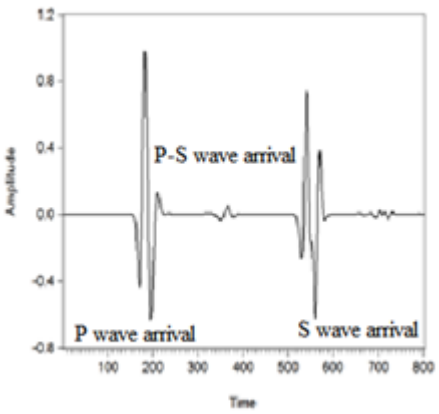

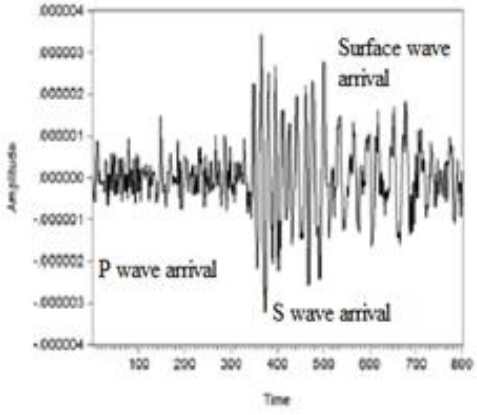

Figure 2: Synthetic trace

Figure 3: Real trace

The descriptive statistics of synthetic and real trace shows general features about the amplitude values of reflection. The average of both traces shows the center of amplitude values that are $1.45e^{-05}$ and 4.06 $e^{-}09$, resectively. After arrainging the amplitude values from lower to higher in synthetic and real trace, the median for synthetic is 0 and for real trace is $-4.26e^{-08}$. Spreadness of values around their means is explained by the measure of dispersion which is known as standard deviation. Synthetic data has the dispersion of 0.149055, however, the real trace has much smaller dispersion in their amplitude values $8.70e^{-07}$. The narrower the standard deviation the closer the midpoint of the data [18]. The skewness describes the asymmetry of reflection or the degree to which the amplitude values are symmetrical around the mean. For normally distributed values skewness is zero as well as the value greater than zero wil exhibit positve skewness and less than zero negative skewness. The positively skewed distribution lies to right and negatively skewed to left. As here, the 1.62143 for gathered trace and 0.184183 real trace value shows that gathered trace from deep explosion source behaves like a positively skewed distribution, while the real trace is not much far away from the normality. Besides the skewness, kurtosis gives the measure of thickness in tails of a distribution. For a normally distributed data, its value is 3 and called mesokurtic. If the value is greater than 3 then leptokurtic and less than 3 called platykurtic distribution. Thus, the value 19.64254 and 4.582009 show platykurtic distributions both in synthetic and real traces, respectively [19].

As the seismic data is a time series data. The fundamental assumption of time series data is independently and identically distributed i.e. *i.i.d* which follows the normal distribution. For example the random walk process which is as follows [20].

$$z_t = z_{t-1} + \epsilon_t \tag{19}$$

where, z_t is any time series. ϵ_t is an i.i.d process; Mean of ϵ_t is $E(\epsilon_t) =$

0 and $Var(\epsilon_t) = E(\epsilon_t{}^2) - E(\epsilon_t)^2 = \sigma^2$ symbolically $\epsilon_t \sim ND(0, \sigma^2)$.

There are three stages in fitting a time series model, identification, estimation and diagnostic checking. In identification stage we decide the order of model, in estimation stage we estimate the model parameters and in last stage, we check the adequacy of fitted model.

The most important tool for identification is the Autocorrelation function (ACF) and Partial Autocorrelation function (PACF). The ACF and PACF are plotted against the lag length and resulting plot is named as correlogram [21].

$$\rho_k = \frac{\varrho_k}{\varrho_o} = \frac{\mathrm{E}[(z_t - \mu)(z_{t+k} - \mu)]}{E(z_t - \mu)^2} \tag{20}$$

$$\varphi_{kk} = \frac{Cov[(z_t - \hat{z}_t)(z_{t+k} - \hat{z}_{t+k})]}{\sqrt{Var(z_t - \hat{z}_{t)}}\sqrt{Var(z_{t+k} - \hat{z}_{t+k)}}} \tag{21}$$

where, ACF and PACF are denoted by ρ_k and φ_{kk}, respectively. z_t is the time series and is its mean μ. k is the lag, ϱ_o is the variance of z_t, ϱ_k is the *kth* covariance of z_t. The PACF between the two series z_t and z_{t+k} is established as the correlation between two mentioned series after removing the linear dependence in these two series. $\hat{z}_t$ and $\hat{z}_{t+k}$ are the linear estimates of z_t and z_{t+k} ,respectively.

The ACF and PACF are plotted against the consecutive time lags and assist in deciding the order of autoregressive (AR) model and moving average (MR) model. It also speaks about the stationarity of series. For stationary series, ACF should have the pattern like sinusoidal wave and PACF should have the sudden death behavior in its lag correlations.

Observing this behavior in ACF and PACF and assuming the first order model feasible for the underlying traces More specifically the Augmented Dickey Fuller (ADF) test explains the stationarity of the data. The ADF test statistic has the value of -6.629117 or synthetic and -13.05380 for real trace. The absolute value of ADF is compared with the critical values at 1%, 5% and 10% level of significance, which are -3.438518, -2.865035, and -2.568686. The value of ADF test is greater in all these cases that infers about the stationarity of data by accepting the alternative hypothesis that there is a no unit root in series. Generally, the time series data have many models and represent the different stochastic process. The two most promising linear time series models are, Autoregressive (AR) and Moving Average (MA) models and the amalgamation of these models are Autoregressive Moving Average (ARMA) models [22]. The MA models are used for the series have trend.

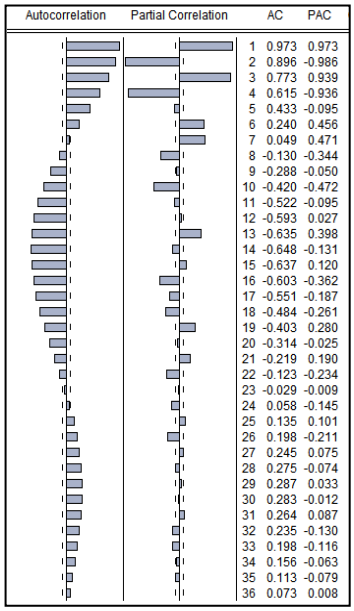

Figure 3: Correlogram of synthetic

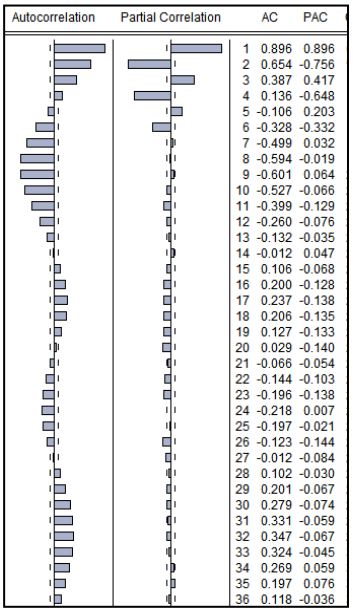

Figure 4: Correlogram of real trace

A real valued stochastic process z_t is said to be an autoregressive process of *pth* order, denoted by AR(p) if there exists $\alpha_1, \alpha_2, \alpha_3, \ldots \alpha_p \in R$ with $\alpha_p \neq 0$ and with a random error, $\epsilon_t \sim ND(0, \sigma^2)$ such that

$$z_t = \alpha_o + \sum_{i=1}^{p} \alpha_p z_{t-p} + \epsilon_t \tag{22}$$

After identifying the parameter *p* for selected model, the next stage is an estimation of the parameters. There are various methods through which we estimate the parameters of any selected model. All of the methods almost give the similar estimates of parameters. They are; ordinary least square (OLS) method, maximum likelihood estimation (MLE) method, the method of moments, and etc [21].Thus, the AR(1) estimated model for synthetic and real data through the OLS estimation are given in equation (23) and (24).

$$z_t = -5.5798e^{-09} + 0.973340 z_{t-1} \tag{23}$$

$$z_t = -1.09173e^{-09} + 0.89691 z_{t-1} \tag{24}$$

In order to find how much variability is explained by the estimated real and synthetic models, we use R^2 measure. The value of R^2 is 94.739% and 80.3855% in synthetic and real models, respectively. it provides enough evidence that AR(1) is fitted good to synthetic and real data. The sum of square of error regression (SSR) talks about the error attributed to the relationship of independent and dependent variable, which is 0.034231 and 3.87e-^{07} and sum of square of error is

0.933894 and $1.19e^{-10}$. The model significance is evaluated by large F-statistic, i.e. 14352.62, and 3262.200 comparing it with the 5% level of significance, -2.86. The Akaike Information criteria (AIC) value -3.908870, and Schwarz information criteria (SIC) -3.897174 for synthetic and well as for real data they are, -26.69464, -26.6829. Though the real data have smaller amplitude values in all descriptive features and model statistics but the explained variation in synthetic data illustrates its goodness of fit.

The testimony of distribution of error for both real and synthetic estimated models is taken by quantiles and correlogram of residuals [19]. The residuals quantiles are around the straight line as shown in Figure 5 and 6. It fulfills the basic assumption of normality of residuals. In Figure 7 and 8 the ACF and PACF of residuals are in their upper and lower band limits values and the randomness of graph depicts the lack of correlation in residuals. [21]

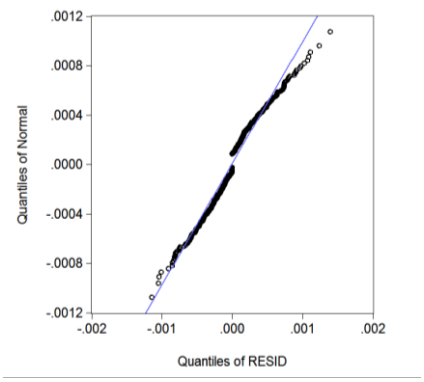

Figure 5: Q-Q plot synthetic data

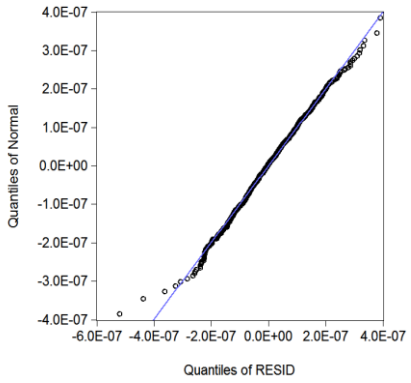

Figure 6: Q-Q plot real data

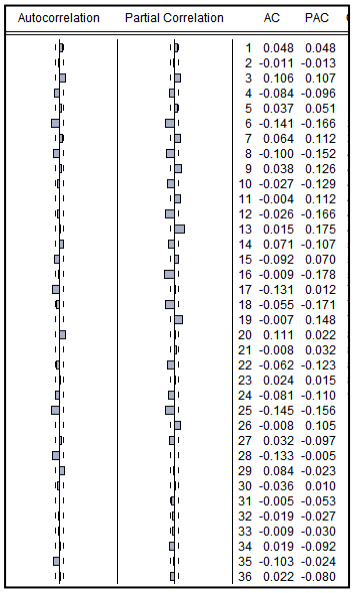

Figure 7: Correlogram of synthetic data residuals

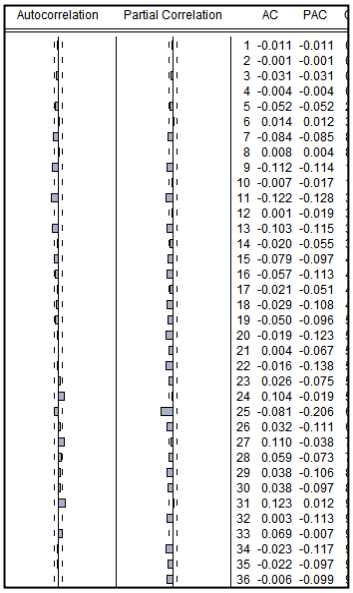

Figure 8: Correlogram of real data residuals

5 Conclusion

On comparing the estimated models in synthetic and real data, the constant terms in these models are similar in their exponents, it is the amplitude value when all the values in predictor are zero, and the slope coefficients are different from zero, so the lag 1 as dependent variable is a helpful predictor. Thus, the autoregressive model of order one models the deep explosive reflections adequately and finite difference method enables the fast and accurate simulation in 2D homogeneous elastic medium. The assuming geological model with the chalk and granite materials and rigid boundary condition helps to predict reservoirs in real data. The synthetic model verifies the subsurface structure in Blackfoot field Alberta Canada. The estimated amplitude value and its concurrence with real model infer the properties of layer because the different materials in subsurface has different reflections.

Acknowledgements. Special thanks to Universiti Teknologi PETRONAS for giving me opportunity to work as graduate research assistant.

References

[1] V. Bokil, "Computational methods for wave propagation problems in unbounded domains," University of Houston, 2003.

[2] B. Alaei, *Seismic modeling of complex geological structures*: INTECH Open Access Publisher, 2012.

[3] C. Sayers and S. Chopra, "Introduction to this special section: Seismic modeling," *The Leading Edge,* vol. 28, pp. 528-529, 2009.

[4] N. C. Wijesinghe, "Seismic Modeling and Imaging of Realistic Earth Models Using New Full-wave Phase-shift Approach," University of Houston, 2014.

[5] J. B. Bednar, "Modeling, Migration and Velocity Analysis in Simple and Complex Structure," *Book,* 2008.

[6] Z. Jiang, "Elastic wave modelling and reverse-time migration by a staggered-grid finite-difference method," 2012.

[7] H. Lan and Z. Zhang, "Comparative study of the free-surface boundary condition in two-dimensional finite-difference elastic wave field simulation," *Journal of Geophysics and Engineering,* vol. 8, p. 275, 2011.

[8] P. Tangtuengtin, "A New Absorbing Boundary Condition Method Using Wavefield Extrapolation," August 8, 2014.

[9] J. Kristek, M. Galis, M. Balazovjech, P. Pazak, and P.Mocozo, "The finite-difference and finite-element modeling of seismic wave propagation and earthquake motion," *Acta physica slovaca,* vol. 57, 2007.

[10] A. C. Parker, "Modelling of seismic wave propagation through realistic and complex fracture networks," TU Delft, Delft University of Technology, 2013.

[11] G. Mavko, "Conceptual Overview of Rock and Fluid Factors That Impact Seismic Velocity and Impedance," *Retrieved,* vol. 11, p. 2012, 2005.

[12] P. Bormann, M. Baumbach, G. Bock, H. Grosser, G. L. Choy, and J. Boatwright, "Seismic sources and source parameters," *IASPEI new manual of seismological observatory practice,* vol. 1, pp. 1-94, 2002.

[13] D. Henley, J. Wong, and P. M. Manning, "Elastic wave 2D modeling of seismic surveys," *the 24th Annual Research Report of the CREWES*

Project, 2012.

[14] J. Yu, "Histogram Matching Seismic Wavelet Phase Estimation," University of Houston, 2012.

[15] M. Bacon, M. Bacon, and R. Simm, *Seismic Amplitude: An Interpreter's Handbook*: Cambridge University Press, 2014.

[16] G. Maslen, "Seismic Reflections," 2013.

[17] C. Cosma, *Vertical and Horizontal Seismic Profiling Investigations at Olkiluoto, 2001*: Posiva, 2003.

[18] G. Marshall and L. Jonker, "An introduction to descriptive statistics: A review and practical guide," *Radiography,* vol. 16, pp. e1-e7, 2010.

[19] R. A. Olea, *A practical primer on geostatistics*: Citeseer, 2009.

[20] E. K. Gathondu, "Modeling of Wholesale Prices for Selected Vegetables Using Time Series Models in Kenya," University of Nairobi, 2014.

[21] D. N. Gujarati, *Basic econometrics*: Tata McGraw-Hill Education, 2012.

[22] R. Adhikari and R. Agrawal, "An Introductory Study on Time Series Modeling and Forecasting," *arXiv preprint arXiv:1302.6613,* 2013.

[23] J. S. Gulati, R. R. Stewart, and J. M. Parkin, "3C-3D VSP: The Blackfoot experiment."

Received: Month xx, 20xx

DETECTION OF LITHOLOGY BY AUTOREGRESSION METHOD

Umairia Malik[1,a)] , Dennis Ling Chuan Ching, Hanita Daud, Vikri Januarisma[2, 3, 4, b,c,d)]

1,2,3 Fundamental and Applied Sciences Department, 4, Electrical and Electronics Engineering Department 32610,Bandar Seri Iskandar, Universiti Teknologi PETRONAS, Malaysia

a)umairiamalik89@gmail.com
b)dennis.ling@petronas.com.my
c)hanita_daud@petronas.com.my
d)vikrijanuarisma@gmail.com

Abstract: Seismic modeling plays an important role in predicting the subsurface lithology. Synthetic model with a fracture is built and discretized using finite difference scheme for spatial and time domain. Common depth point (CDP) with single shot gives traces and automatic gain is preprocessed before fitting an Autoregressive (AR) model. A comparison of synthetic data in the presence of Clayton Engquist (CE) boundary condition and BF-data is performed on the basis of a mean square error of AR model. The BF-data has a minimum means square error. Conclusively, the CE boundary doesn't absorb the seismic reflections completely.

INTRODUCTION

The active and passive geophysical methods respond to the physical properties of subsurface such as rocks, water, sediments and etc. The active geophysical methods are used for seismic exploration, in which the artificial signals are penetrated into the subsurface and seismic energy strike the boundaries between contrasting materials at normal incidence. This energy undergoes a partial reflection at the interface with different physical properties, especially density and remaining is transmitted into deeper layers. Seismic source, seismograph and a series of geophones to detect the arrival of seismic waves are the three key components for conducting a seismic reflection profiling. The reflected seismic waves are recorded by geophones at the surface and termed as seismic trace [1].

The simulated seismic reflectivity series are used to image the subsurface structures and modeled as a sequence of reflection coefficients that have fundamental importance for seismic interpretation. A paper by Walden and Hosken showed that primary reflections could be modeled as autoregressive moving average method [2]. For modeling the seismic reflection [3] used the six order autoregressive (AR) model for a well-log data. Furthermore, a two stage autoregressive (AR) extrapolation approach is employed to extend the amplitude spectrum by [4]. Determination of appropriate AR model from vast seismic data has been a key concerned for researchers as mention [5]. Autoregressive model based algorithm is presented by [6] for automatic detection of S-phase arrival. A scalar AR model predicts the horizontal components of waveforms.

The oil, gas and other valuable minerals are explored by seismic exploration methods. The recorded seismic data allow drawing a conclusion about the subsurface structure and lithological compositions. Amplitude scaling is a preprocessing step before any further processing is employed on synthetic gathers. It is difficult to interpret the results as the different rock layers affect the wave propagation in terms of their amplitude variation. Usually, the traces near the surface have strong amplitudes at early times while at far-offset traces synthetic data have weak and non-existent reflections. For simply mapping the amplitude, an easy way is to apply the automatic gain control (AGC). Its objective is to scale the synthetic data such that in a sliding window average value of the amplitude is calculated inside the window [7]. In a context of wave propagation, fractures are explained as thin layers, linear slip or interfaces in the subsurface. The occurrence of these discontinuities or fractures in reservoirs and non-reservoirs can have a strong influence on imaging the subsurface structure. They affect response in the isotropic medium, velocity, and amplitude. The interpretation of the synthetic model in terms of reservoirs can be used to extrapolate the actual reservoirs in the earth. Thus, modeling the seismic reflections by using the Autoregressive (AR) model is a proposed idea in this paper.

METHODOLOGY

The seismic method employs the propagation of waves throughout the earth to locate the stratigraphy and structures as elastic properties will change with depth. In exploration seismology, understanding of wave propagation is an important point and hence seismic modeling is an important tool [8]. There are two ways to find the physical parameters in the subsurface either by forward modeling or inversion modeling. In forward modeling, a geophysical model is constructed according to particular physical properties such as the velocity of primary and secondary or shear wave and density. However, its converse is inversion modeling [9]. Finite difference method is widely used for modeling the seismic wave propagation and provides the complete image of wave field at each point in the model for every time step. Implicit and explicit are two formulations in finite difference method. In explicit the wavefield at the present time is estimated by using the wavefield at past time but in implicit the present values of wavefield depend on the past and future values [10].

2D P-SV Wave Modeling

The 2D seismic wave equation in isotropic medium is as follows [11]:

$$\rho(x)\frac{\partial^2 U(x,t)}{\partial t^2} = \frac{\partial}{\partial x_j}\left[\left\{\lambda\delta_{ij}\left(\frac{\partial u_k}{\partial x_k}\right) + \mu\left(\frac{\partial u_i(x,t)}{\partial x_j} + \frac{\partial u_j(x,t)}{\partial x_i}\right)\right\}\right] \qquad i,j=1,2 \tag{1}$$

$$\mu = \frac{\tau_{ij}}{2\varepsilon_{ij}} \tag{2}$$

$$\tau_{ij}(x,t) = C_{ijkl}(x)\varepsilon_{kl}(x,t) + I_{ij}(x,t) \qquad i,j,k,l=1,2,3 \tag{3}$$

$$C_{ijkl} = \lambda\delta_{ij}\delta_{kl} + \mu(\delta_{il}\delta_{jk} + \delta_{ik}\delta_{jl}) \tag{4}$$

$$\varepsilon_{ij} = \frac{1}{2}\left(\frac{\partial u_i(x,t)}{\partial x_j} + \frac{\partial u_j(x,t)}{\partial x_i}\right) \quad i,j=1,2 \tag{5}$$

$$\left.\begin{array}{l}\delta_{ij} = 1 \quad if \;\; i = j \\ \delta_{ij} = 0 \quad if \;\; i \neq j\end{array}\right\} \tag{6}$$

where: $\rho(x) = \rho$ is the density, $U(x,t) = U$ are the displacement components, λ and μ are Lamé parameters of material, τ_{ij} is stress tensor, δ is called Kronecker delta function, $\varepsilon = \varepsilon_{kl}(x,t)$, these strains represent the compression of rocks under high pressure, $C = C_{ijkl}(x)$ is elastic tensor and $I = I_{ij}(x,t)$, represents external stresses. By solving the equation (1), we get the velocities of P and S waves and as follows:

$$V_p = \sqrt{\frac{\lambda+2\mu}{\rho}} \tag{7}$$

$$V_s = \sqrt{\frac{\mu}{\rho}} \tag{8}$$

The above seismic wave equations in velocity-stress system are presented as follows [12]:

$$\rho\frac{\partial v_1}{\partial t} = \frac{\partial \tau_{11}}{\partial x_1} + \frac{\partial \tau_{13}}{\partial x_3} \tag{9}$$

$$\rho\frac{\partial v_3}{\partial t} = \frac{\partial \tau_{13}}{\partial x_1} + \frac{\partial \tau_{33}}{\partial x_3} \tag{10}$$

$$\frac{\partial \tau_{11}}{\partial t} = (\lambda + 2\mu)\frac{\partial v_1}{\partial x_1} + \lambda\frac{\partial v_3}{\partial x_3} \tag{11}$$

$$\frac{\partial \tau_{33}}{\partial t} = (\lambda + 2\mu)\frac{\partial v_3}{\partial x_3} + \lambda\frac{\partial v_1}{\partial x_1} \tag{12}$$

$$\frac{\partial \tau_{13}}{\partial t} = \mu\left(\frac{\partial v_1}{\partial x_3} + \frac{\partial v_3}{\partial x_1}\right) \tag{13}$$

where: v_1 and v_3 are horizontal and vertical velocities , τ_{11}, τ_{33} τ_{13} and are stress tensors in x_1 , x_3 and x_{13} directions, respectively.
If the grid size is h for both x_1 and x_3 axes and Δt is the time step, then the approximations of velocity-stress system of equations are formulated according to the Virieux method from equations (9) to (13).

$$\rho\left(\frac{{v_1}_{i,k}^{n+\frac{1}{2}}-{v_1}_{i,k}^{n-\frac{1}{2}}}{\Delta t}\right)=\left\{\left(\frac{{\tau_{11}}_{i+\frac{1}{2},k}^{n}-{\tau_{11}}_{i-\frac{1}{2},k}^{n}}{h}\right)+\left(\frac{{\tau_{13}}_{i,k+\frac{1}{2}}^{n}-{\tau_{13}}_{i,k-\frac{1}{2}}^{n}}{h}\right)\right\} \tag{14}$$

$$\rho\left(\frac{{v_3}_{i+\frac{1}{2},k+\frac{1}{2}}^{n+\frac{1}{2}}-{v_3}_{i+\frac{1}{2},k+\frac{1}{2}}^{n-\frac{1}{2}}}{\Delta t}\right)=\left\{\left(\frac{{\tau_{13}}_{i+1,k+\frac{1}{2}}^{n}-{\tau_{13}}_{i,k+\frac{1}{2}}^{n}}{h}\right)+\left(\frac{{\tau_{33}}_{i+\frac{1}{2},k+1}^{n}-{\tau_{33}}_{i+\frac{1}{2},k}^{n}}{h}\right)\right\} \tag{15}$$

$$\left(\frac{{\tau_{11}}_{i+\frac{1}{2},k}^{n+1}-{\tau_{11}}_{i+\frac{1}{2},k}^{n}}{\Delta t}\right)=\left\{(\lambda+2\mu)_{i+\frac{1}{2},k}\left(\frac{{v_1}_{i+1,k}^{n+\frac{1}{2}}-{v_1}_{i,k}^{n+\frac{1}{2}}}{h}\right)+\lambda_{i+\frac{1}{2},k}\left(\frac{{\tau_{33}}_{i+\frac{1}{2},k+\frac{1}{2}}^{n+\frac{1}{2}}-{\tau_{33}}_{i+\frac{1}{2},k-\frac{1}{2}}^{n+\frac{1}{2}}}{h}\right)\right\} \tag{16}$$

$$\left(\frac{{\tau}_{i+\frac{1}{2},k}^{n+1}-{\tau_{33}}_{i+\frac{1}{2},k}^{n}}{\Delta t}\right)=\left\{(\lambda+2\mu)_{i+\frac{1}{2},k}\left(\frac{{\tau_{33}}_{i+\frac{1}{2},k+\frac{1}{2}}^{n+\frac{1}{2}}-{\tau_{33}}_{i+\frac{1}{2},k-\frac{1}{2}}^{n+\frac{1}{2}}}{h}\right)+\lambda_{i+\frac{1}{2},k}\left(\frac{{v_1}_{i+1,k}^{n+\frac{1}{2}}-{v_1}_{i,k}^{n+\frac{1}{2}}}{h}\right)\right\} \tag{17}$$

$$\left(\frac{{\tau_{13}}_{i,k+\frac{1}{2}}^{n+1}-{\tau_{13}}_{i,k+\frac{1}{2}}^{n}}{\Delta t}\right)=\left\{\mu_{i,k+\frac{1}{2}}\left(\frac{{v_3}_{i+\frac{1}{2},k+\frac{1}{2}}^{n+\frac{1}{2}}-{v_3}_{i-\frac{1}{2},k+\frac{1}{2}}^{n+\frac{1}{2}}}{h}+\frac{{v_1}_{i+1,k}^{n+\frac{1}{2}}-{v_1}_{i,k}^{n+\frac{1}{2}}}{h}\right)\right\} \tag{18}$$

The above equations are solved under the initial conditions:

$$\frac{\partial v_1}{\partial t}=0 \tag{19}$$

$$\frac{\partial v_3}{\partial t}=0 \tag{20}$$

$$\frac{\partial \tau_{11}}{\partial t}=0 \tag{21}$$

$$\frac{\partial \tau_{13}}{\partial t}=0 \tag{22}$$

$$\frac{\partial \tau_{33}}{\partial t}=0 \tag{23}$$

The finite difference approximations of these initial conditions are elaborated for equation (19) to (23), respectively:

$$\frac{{v_1}_{i,k}^{n+\frac{1}{2}}-{v_1}_{i,k}^{n-\frac{1}{2}}}{\Delta t}=0 \tag{24}$$

$$\frac{{v_3}_{i+\frac{1}{2},k+\frac{1}{2}}^{n+\frac{1}{2}}-{v_3}_{i+\frac{1}{2},k+\frac{1}{2}}^{n-\frac{1}{2}}}{\Delta t}=0 \tag{25}$$

$$\frac{{\tau_{11}}_{i+\frac{1}{2},k}^{n+1}-{\tau_{11}}_{i+\frac{1}{2},k}^{n}}{\Delta t}=0 \tag{26}$$

$$\frac{{\tau_{13}}_{i,k+\frac{1}{2}}^{n+1}-{\tau_{13}}_{i,k+\frac{1}{2}}^{n}}{\Delta t}=0 \tag{27}$$

$$\frac{\tau_{i+\frac{1}{2},k}^{n+1} - \tau_{33}{}_{i+\frac{1}{2},k}^{n}}{\Delta t} = 0 \tag{28}$$

In order to prevent the unwanted artifacts from the boundaries, Lindman [13], Engquist and Majda [14] initiated the absorbing boundary conditions. In Clayton Engquist (CE) boundary condition, actual wave equations are damped by paraxial approximations which don't allow the energy from the boundary to propagate back to the numerical mesh. The outward boundary is filled with approximations thus, the solution of the interior is extrapolated [15].

The boundary condition, Clayton Engquist for the above velocity-stress system is as follows:

$$\frac{\partial v_1}{\partial x_1} + \frac{1}{V_S}\frac{\partial v_1}{\partial t} = 0 \tag{29}$$

$$\frac{\partial v_3}{\partial x_3} + \frac{1}{V_P}\frac{\partial v_3}{\partial t} = 0 \tag{30}$$

The finite difference approximation for these equations (29) and (30) are as follows:

$$\left(\frac{v_1{}_{i+1,k}^{n} - v_1{}_{i,k}^{n}}{h}\right) + \frac{1}{Vs}\left(\frac{v_1{}_{i,k}^{n+\frac{1}{2}} - v_1{}_{i,k}^{n-\frac{1}{2}}}{\Delta t}\right) = 0 \tag{31}$$

$$\left(\frac{v_3{}_{i+\frac{1}{2},k+\frac{1}{2}}^{n+\frac{1}{2}} - v_3{}_{i+\frac{1}{2},k-\frac{1}{2}}^{n+\frac{1}{2}}}{h}\right) + \frac{1}{Vp}\left(\frac{v_3{}_{i+\frac{1}{2},k+\frac{1}{2}}^{n+\frac{1}{2}} - v_3{}_{i+\frac{1}{2},k+\frac{1}{2}}^{n-\frac{1}{2}}}{\Delta t}\right) = 0 \tag{32}$$

As the generated synthetic data in forward modeling is a time series data. The time series data is defined as a set of vectors $y(t), t = 0,1,2,\ldots$[16]. Simply the Autoregressive (AR) model of order 1 is defined in equation (33).

$$y_t = \alpha_o + \alpha_1 y_{t-1} + \epsilon_t \tag{33}$$

where: mean and variance of AR(1) is $\mu = \frac{\alpha_o}{1-\alpha_1}$ and $V(y_t) = \frac{\sigma^2}{1-\alpha_1{}^2}$, respectively.

RESULTS AND DISCUSSIONS

The CREWES mfD2D package is used for simulation that is based on the 2D P-SV wave modeling. In order to investigate the wave propagation into the subsurface structure a single shot with the split end geometry is taken, where receivers are placed on both sides of sources. There are total thirty receivers in a diagonal reflector model which is 2000 m long in the *x*-axis and 1000 m wide in *z*-axis. The first shot is taken at 1000 m in length, 10 m in depth and the reflector is introduced at 800 m depth. The P wave velocity must be in (1000 m/s to 5000 m/s), S-wave velocity (500 m/s to 3500 m/s) and density in 1.0 to 2.7 [17]. Different materials have different velocities in the mentioned range and density that affect the reflectivity from subsurface layers. Here, the layers are assigned the velocities and density according to the shales and marls material, respectively. For the upper layer, the P-wave velocity is set to 2500 (m/s), S-wave velocity 800 (m/s) and density of the first layer is 2 (g/cm^3). For the second layer velocity of P-wave is 3000 (m/s), S-wave velocity is 1500 (m/s) and density 2.2 (g/cm^3). A stable criterion for checking the P and S velocities are in range is Poisson's ration. The Poisson's ratio must be less than 0.707. The shot spacing is 25 m in length while there is zero spacing in depth and consequently, the grid size is 2.5m. Furthermore, minimum phase wavelet with a center frequency of 30 Hz is used as the source in modeling. The time step is chosen according to the stability condition as mention in equation (34) and it is 0.0002 seconds (s) and receivers record the reflections after each time step. The total recording time is 0.8 seconds (s). The absorbing boundary condition CE is used in all four edges of the model domain that helps to solve the finite difference equations at the edges of the model.

$$\Delta t < \sqrt{2}\frac{\Delta x}{V_{max}} \tag{34}$$

where: Δt is the time step, Δx is the grid size and V_{max} is the highest velocity in the model i.e. 3000 (m/s). The waves are propagated into subsurface by forward modeling; the receivers on the subsurface record these waves. Figure. 1 describes the velocity model of shale and marls material, while Figure.2 explains the gathered traces in a horizontal seismic profile data. The weak reflections are enhanced by using the Automatic Gain Control (AGC) scaling function.

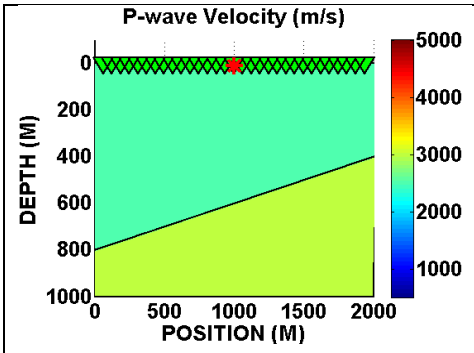

Figure 1. Velocity Model

The synthetic and real data reflections are modeled by using the first order autoregression and a comparison is carried by using the means square error (MSE). The goodness of fit measure i.e. R^2 of real and synthetic data indicates that seismic reflections can be modeled by AR.

The AR equation for synthetic data is as follows:

$$y_t = 1.6721e^{-02} + 0.98745y_{t-1} \tag{35}$$

With SSE= 0.153528, R^2=0.97508, adjusted R^2= 0.97508 and MSE =0.0002074. The term $1.6721e^{-02}$ indicates the average reflectivity in the presence of specified materials, the 0.98745 is different from zero, so the lag 1 variable is a predictor and. R^2 has the range of $0 \leq R^2 \leq 1$, shows how much variability has been explained by the fitted model, the nearer to 1 the better the fitted model, however in the presence of noise it cannot be near to 1 or below the zero indicates that model is not fitted well to the data. MSE measures of how close a fitted line is to data points. But in the present case, it is nearer to 1 that shows the goodness of fit of the model. Now the equation for real data is as follows:

$$y_t = -1.80e^{-10} + 0.96946y_{t-1} \tag{36}$$

With SSE= $2.33e^{-11}$, R^2= 0.939741, adjusted R^2=0.93966 and MSE = $1.71e^{-7}$. On the basis of results, the real data has smaller MSE as compare to synthetic data. The intercept terms of real and synthetic data are different but the coefficients of y_t proves that the AR(1) is appropriate model. If the intercept terms i.e. the average reflectivity, are similar then we can say that our real and synthetic models have similar lithology that shows the rock types. There are following reasons that may affect the lithology such as boundary conditions, scaling function in AGC and velocities of layers because different velocity layers have different reflections. It also concludes that CE boundary condition doesn't absorb the seismic reflections completely. The other boundary conditions, material velocities and, gain functions can be checked which could have less seismic reflections from boundaries of model and have more nearer results to real data.

ACKNOWLEDGEMENTS

The corresponding author would like to thanks, Universiti Teknologi PETRONAS for the Graduate Assistantship and financial support.

REFERENCES

[1] J. M. Reynolds, *An introduction to applied and environmental geophysics*: John Wiley & Sons, 2011.
[2] K. Helbig, *Modeling the Earth for Oil Exploration: Final Report of the CEC's Geoscience I*: Elsevier, 2015.
[3] R. Aggarwal, M. P. Lamoureux, and G. F. Margrave, "Modelling and simulation of seismic reflectivity," *CREWES Research Report,* vol. 14, pp. 1-10, 2002.
[4] S. Dasgupta and R. L. Nowack, "Frequency extrapolation to enhance the deconvolution of transmitted seismic waves," *Journal of Geophysics and Engineering,* vol. 5, p. 118, 2008.
[5] I. B. MacNeill and G. Umphrey, *Time Series and Econometric Modelling: Advances in the Statistical Sciences: Festschrift in Honor of Professor VM Joshi's 70th Birthday* vol. 3: Springer Science & Business Media, 2012.
[6] L. Küperkoch, T. Meier, A. Brüstle, J. Lee, and W. Friederich, "Automated determination of S-phase arrival times using autoregressive prediction: application to local and regional distances," *Geophysical Journal International,* vol. 188, pp. 687-702, 2012.
[7] R. Simm, M. Bacon, and M. Bacon, *Seismic Amplitude: An interpreter's handbook*: Cambridge University Press, 2014.
[8] M. Nejati and H. Hashemi, "Migrated Exploding Reflectors in Evaluation of Finite Difference Solution for Inhomogeneous Seismic Models," 2012.
[9] N. H. Hussain, "A Study Of Marine CSEM Survey Geometry For Seabed Logging," Universiti Teknologi PETRONAS, 2011.
[10] B. Alaei, *Seismic modeling of complex geological structures*: INTECH Open Access Publisher, 2012.
[11] P. M. Shearer, *Introduction to seismology*: Cambridge University Press, 2009.
[12] Z. Jiang, "Elastic wave modeling and reverse-time migration by a staggered-grid finite-difference method," University of Calgary, 2012.
[13] E. Lindman, "“Free-space” boundary conditions for the time dependent wave equation," *Journal of computational physics,* vol. 18, pp. 66-78, 1975.
[14] B. Engquist and A. Majda, "Absorbing boundary conditions for numerical simulation of waves," *Proceedings of the National Academy of Sciences,* vol. 74, pp. 1765-1766, 1977.
[15] N. A. Petersson and B. Sjogreen, "An energy absorbing far-field boundary condition for the elastic wave equation," *Communications in Computational Physics,* vol. 6, p. 483, 2009.
[16] R. Adhikari and R. Agrawal, "An introductory study on time series modeling and forecasting," *arXiv preprint arXiv:1302.6613,* 2013.
[17] J. Wong, P. M. Manning, and D. Henley, "Elastic wave 2D modeling of seismic surveys," *the 24th Annual Research Report of the CREWES Project,* 2012.